Evaluation of geochemical and hydrogeological processes by geochemical modeling in an area affected by evaporite karstification

P. Acero[a,1,*], L. F. Auqué[a], J. P. Galve[a], F. Gutiérrez[a], D. Carbonel[a], M. J. Gimeno[a], Y. Yechieli[b], M.P. Asta[a,c] and J. B. Gómez[a]

[a] Earth Sciences Department, University of Zaragoza, c/ Pedro Cerbuna 12, 50009, Zaragoza, Spain.

[b] Geological Survey of Israel, 30 Malkhei Israel Street, Jerusalem 95501, Israel and Department of Environmental Hydrology & Microbiology, Zuckerberg Institute for Water Research, Blaustein Institutes for Desert Studies, Ben Gurion University of the Negev, Sede Boqer, Israel.

[c] Instituto Andaluz de Ciencias de la Tierra (IACT) (CSIC-UGR), Avda. de las Palmeras, 4; 18100 Armilla, Granada, Spain.

[1] Present address: Earth and Planetary Science Department, Birkbeck, University of London, Malet Street, WC1E 7HX London, United Kingdom.

*corresponding author: patri.acero@gmail.com. Tel: +34 976 761067 / +447851946528/ Fax: +34 976 761106.

Submitted to Journal of Hydrology

8 Figures

5 Tables

1 Electronic Annex

Abstract

A combination of inverse (mixing + mass-balance) and forward (reaction-path) geochemical calculations is applied for the quantification of the main processes and seasonal variations in an area severely affected by evaporite karstification (Ebro Valley in the outskirts of Zaragoza city; NE Spain). The obtained results prove the suitability of the applied methodology to the characterisation of similar problems in other areas with scarce geological and hydrogeological information.

The hydrogeology and hydrochemistry of the system can be mainly attributed to the mixing of variable proportions of concentrated groundwater from the evaporitic aquifer and more dilute water from the overlying alluvial aquifer. The existence of a good connection between these aquifers is supported by: 1) the fast changes in the hydrochemistry of the karst aquifer to recharge by irrigation, and 2) the deduced input of evaporitic groundwater in the alluvial materials. The evolution in some parts of the alluvial/evaporitic aquifer system is clearly dominated by the seasonal variations in the recharge by dilute irrigation waters (up to 95% of water volume in some sinkhole ponds), whereas other points seem to be clearly determined by the hydrochemistry of the concentrated evaporitic aquifer groundwater (up to 50% of the water volume in some springs).

The following reactions, previous or superimposed to mixing processes, explain the observed hydrochemistry in the studied area: dissolution of halite (NaCl), gypsum ($CaSO_4 \cdot 2H_2O$)/anhydrite ($CaSO_4$) and dolomite ($CaMg(CO_3)_2$), CO_2(g) input and degassing and calcite ($CaCO_3$) dissolution/precipitation. The modeling results suggest the existence of a large spatial variability in the composition of the evaporitic groundwater, mainly caused by large differences in the availability of halite in contact with the groundwater.

47 Active subsidence associated with halite dissolution is expected to continue in the study
48 area, together with the episodic increase of gypsum dissolution associated with the input
49 of dilute irrigation waters.

50 **Keywords:** hydrochemistry, mixing, sinkholes, mass-balance calculations.

51

52 **1- INTRODUCTION**

53 In karst terrains, subsurface dissolution of carbonate and/or evaporitic materials by
54 groundwater may lead to the gravitational instability and internal erosion of the
55 overlying sediments, eventually resulting in the settlement of the ground surface (e.g.
56 Waltham et al., 2005; Gutiérrez, 2010). This subsidence hazard may constitute a
57 significant limitation for development and may lead to high risk scenarios in areas with
58 human structures and activities, causing significant direct and indirect economic losses
59 (Gutiérrez *et al*., 2008a).

60 Mitigating the sinkhole risk in a cost-effective way requires a detailed knowledge on the
61 processes and factors involved in karstification. Among other features, the mineralogy,
62 hydrochemistry and hydrogeology of the target areas need to be well-known in order to
63 understand the processes leading to sinkhole development (Lamont-Black *et al*., 2002).
64 However, a drawback commonly encountered for the detailed characterization of these
65 types of processes in many evaporite karst systems is the scarcity of appropriate
66 boreholes providing direct information from the target geologic materials and the
67 associated groundwater.

68 In order to overcome this limitation, a cost-effective approach that can be applied to
69 infer a general hydrogeological model and the associated geochemical processes,
70 including karstification, is the analysis of hydrochemical information and geochemical
71 calculations. This methodology has been extensively applied in many karst aquifers
72 aimed at identifying flow patterns, calculating mixing ratios, identifying geochemical
73 reactions along groundwater flow-paths and pinpointing hydraulic connections between
74 aquifers. Nevertheless, the vast majority of earlier works dealing with karst
75 hydrogeology and geochemistry have been carried out in carbonate aquifers (Plummer

76 *et al*., 1990; Lee and Krothe, 2001; López-Chicano *et al*., 2001; Uliana and Sharp,
77 2001; Wang and Luo, 2001; Aquilina *et al*., 2003, 2005, 2006 and references therein;
78 Barbieri *et al*., 2005; Tuccimei *et al*., 2005; Moral *et al*., 2008; Auqué *et al*., 2009;
79 Moore *et al*., 2009; Belkhiri *et al*., 2010; Dassi, 2011; Barberá and Andreo, 2012 and
80 references therein; Bicalho *et al*., 2012; Carucci *et al*., 2012; Huang and Chen, 2012 and
81 references therein; Wong *et al*., 2012; Markovic *et al*., 2013; Xie *et al*., 2013), whereas
82 the works focused on evaporite karst systems are much more scarce (Kaçaroglu *et al*.,
83 2001; Günay, 2002; Land, 2003; Lamont-Black *et al*., 2005; Yechieli *et al*., 2006;
84 Omelon *et al*., 2006; Chiesi *et al*., 2010; Fidelibus *et al*., 2011; Apaydin and Aktas,
85 2012). Moreover, in spite of the large potential of mass-balance and reaction-path
86 geochemical calculations to shed light on the hydrogeological and geochemical
87 processes in karst systems, this methodology has not been applied, to our knowledge, to
88 any evaporite karst system.

89 Thus, the main goal of this study is to explore the practicality of hydrochemical data
90 and the application of geochemical modeling to quantify the relative importance of the
91 different processes involved in evaporite karstification and to assess the role of their
92 seasonal variations. This approach has been applied to a stretch of the Ebro Valley
93 alluvial evaporite karst, including Zaragoza city (NE Spain). Even though this is one of
94 the areas in the world where subsidence risk related to evaporite dissolution has the
95 greatest economic impact (Gutiérrez *et al*., 2008a; Galve *et al*., 2009) and where more
96 studies on evaporite karst subsidence have been published (Gutiérrez et al., 2007,
97 2008a; Castañeda et al., 2009; Galve et al., 2009; Guerrero et al., 2013), a detailed
98 assessment of the hydrogeochemical and hydrogeological processes behind these highly
99 hazardous phenomena has not been carried out yet. The interpretation of modeling
100 results will allow identifying differences in the hydrogeology and mineralogy of

101 different portions of the studied system and some of the main current uncertainties
102 about the Ebro Valley alluvial evaporite karst.

103

104 **2- STUDY AREA**

105 **2.1- Geological setting and climate**

106 The studied area is a 60 km-long reach of the Ebro River valley located in the central
107 sector of the Ebro Tertiary Basin (NE Spain), which constitutes the southern foreland
108 basin of the Pyrenees (Fig. 1). In this section of the Ebro Valley, the river has been
109 carved in subhorizontally lying evaporites of the Oligo-Miocene Zaragoza Formation
110 (Quirantes, 1978, Ortí and Salvany, 1997). In the subsurface, the formation is primarily
111 composed of anhydrite ($CaSO_4$)/gypsum ($CaSO_4 \cdot 2H_2O$), halite (NaCl) and glauberite
112 ($Na_2Ca(SO_4)_2$), with interlayered marls and lutites including calcite ($CaCO_3$), dolomite
113 ($CaMg(CO_3)_2$) and quartz (SiO_2) (Salvany *et al*., 2007 and references therein; Guerrero
114 *et al*., 2008a,b, 2013). In outcrop, the evaporitic succession exhibits around 300 m of
115 laminated and nodular secondary gypsum derived from the hydration of anhydrite or
116 from the replacement of glauberite. The evaporitic formation changes laterally into
117 impervious and insoluble clay facies, which probably act as a hydrogeological barrier
118 for the evaporite karst aquifer in the eastern (downstream) sector of the studied area
119 (Fig. 1b). In the studied reach of the valley, the terrace and pediment deposits overlying
120 the evaporitic materials may reach 80 m in thickness and fill basins several kilometers
121 long generated by dissolution-induced synsedimentary subsidence (Guerrero *et al*., 2013
122 and references therein). These alluvial deposits mainly consist of gravels dominated by
123 siliciclastic and carbonate pebbles with a sand-silt matrix, commonly cemented by
124 carbonates.

125 (insert here Figure 1)

126 Sinkholes derived from the karstification of the evaporitic materials are a common
127 geomorphological feature in the area. Some sinkholes in the valley bottom are

permanently filled with water (Fig. 2) and, therefore, may provide information on the hydrochemical and hydrogeological features of the alluvial-karst aquifer system.

(insert here Figure 2)

The climate in this region is Mediterranean with strong continental influence, characterized by hot summers and cold winters. The mean monthly temperature ranges from 9 ºC to 21ºC (Ninyerola *et al*., 2005). The average annual precipitation in the Zaragoza area is around 340 mm and it shows a considerable inter-annual variability. A significant proportion of the precipitation corresponds to intense, short-duration convective storms that commonly occur in spring and autumn. The year 2011, corresponding to the sampling campaign specifically carried out for this study, showed a total precipitation of 315 mm, indicating a slightly dryer year in relation to the average. The mean annual reference evapotranspiration in Ebro Valley exceeds 1150 mm, indicating a negative water balance of more than 800 mm and, therefore, a climate characterized by semiarid conditions (Diputación General de Aragón, 2007).

2.2- Hydrogeology

Two main interconnected aquifers can be identified in the study area: (1) the alluvial aquifer, composed by the alluvium underlying the valley bottom and the associated terrace deposits at the valley margins; (2) the karst aquifer developed in the evaporitic bedrock. The effluent Ebro River and the associated valley bottom alluvium acts as the base level for the alluvial-karst aquifer system and the general flow direction in the alluvial aquifer is developed towards the river (Fig. 1). The largest proportion of water input to the system in the studied stretch of the valley is anthropogenic induced recharge in the urban area of Zaragoza and irrigation, which represents more than 90% of the groundwater input (Durán *et al*., 2005). The main irrigation sources are the Ebro River,

the Imperial Canal and the Urdana ditch (Fig. 1a and b). Irrigation processes are the main cause of the seasonal variations in the water table, which may rise several meters by the end of the irrigation season (around September), when the river flow is commonly low.

Although the hydrogeological information about the evaporite karst aquifer is scarce, multiple lines of evidence suggest that it has a considerable permeability due to dissolution processes (Gutiérrez *et al*., 2007, Guerrero *et al*., 2008b, 2013; Galve *et al*., 2009). The recharge of the evaporitic aquifer is thought to occur through infiltration of irrigation and precipitation water in the bedrock outcrops and perched alluvial deposits. The groundwater that flows through the salt-bearing evaporitic bedrock progressively increases its concentrations of total dissolved solids (TDS) and ultimately discharges into the floodplain alluvium, as evidenced by the frequent presence in this aquifer of highly-saline waters associated with springs, wells and sinkhole ponds. Some authors have proposed that there may be areas of preferential discharge of the evaporite karst aquifer into the overlying alluvial aquifer (Jiménez-Torrecilla *et al*., 2004; Sánchez *et al*., 2004; Gutiérrez *et al*., 2007).

3- METHODOLOGY

3.1- Selection of water points for hydrochemical characterisation

Time series of hydrochemical data from 23 sampling points (wells, springs, sinkhole ponds, ditches and the Ebro River; Table 1) were included in this study to characterize the main hydrochemical features of the Ebro alluvial aquifer and to explore its relationship with the evaporitic karst aquifer in the study area. As displayed in Table 1, the hydrochemical information from some of the points could be obtained from the public database of the Ebro Water Authority (Confederación Hidrográfica del Ebro;

176 CHE). For the rest of the sampling points, 3 to 7 sampling surveys were carried out
177 between January 2011 and January 2012. Apart from these new sampling points, some
178 additional samples were also collected during the surveys for analysis at some of the
179 points from the CHE database in order to confirm and complete their reported
180 hydrochemistry. A systematic nomenclature has been used for the sampling points in
181 order to facilitate the understanding of the results and interpretations (see explanation in
182 Table 1). To facilitate the interpretations, the study area has been divided into two
183 zones: Zone 1 for the sampling points located W of Zaragoza city and Zone 2 for the
184 points placed E of Zaragoza city (Fig. 1a).

185 As displayed in Table 1, two of the wells withdraw groundwater from the evaporitic
186 aquifer (1WA2 and 2WA7, for zone 1 and 2, respectively), whereas the rest of them
187 withdraw water from depths corresponding to the alluvial aquifer (Table 1), although
188 they may be also affected by variable mixing with the evaporitic aquifer groundwater.
189 In the case of springs, their aquifer association is uncertain and will be assessed on the
190 basis of their hydrochemistry.

191 (insert here Table 1)

192 **3.2- Methods for sampling, analysis and geochemical modeling**

193 The methods for sampling and analysis have been extensively described elsewhere
194 (Acero *et al.*, 2013). The hydrochemistry of the studied points was studied in samples
195 obtained by pumping (in wells) or manually (in springs, ponds, ditches and in the Ebro
196 River). Temperature, conductivity and pH were determined in the field and the
197 alkalinity and concentrations of Cl, SO_4, Ca, Mg, Na, K, Sr and Si were measured in the
198 laboratory by different methods (see Acero *et al*., 2013 for further details).

199 Geochemical calculations that will be discussed throughout this work have been
200 performed with the PHREEQC code (Parkhust and Appelo, 2013) using the WATEQ4F
201 thermodynamic database (Ball and Nordstrom, 2001) included in the PHREEQC
202 package. The calculated charge balance error for the reported analyses, as calculated
203 with the PHREEQC code, is generally below 5% and never above 10%.

204

205 **4- RESULTS AND DISCUSSION**

206 In this section, the results obtained from different plots and calculations are presented
207 and discussed. Firstly, the general hydrochemical features and seasonal variations of the
208 studied zones are explored and the main hydrogeological and geochemical processes
209 already identified in Acero *et al.* (2013) are briefly detailed. Secondly, the identified
210 processes are combined into several conceptual models and tested with the assistance of
211 inverse (mixing + mass-balance) and forward (reaction-path) geochemical calculations.

212 **4.1- General hydrochemical features and seasonal variations**

213 For the characterization of the general hydrochemical features of the alluvial-karst
214 system in the surroundings of Zaragoza city, and in order to maximize the
215 representativeness of the data, the whole hydrochemical dataset (i.e. data from the Ebro
216 Water Authority plus data from our sampling campaigns; Table EA1 in the electronic
217 annex) has been used.

218 There are some common hydrochemical features for Zone 1 (W of Zaragoza city) and
219 Zone 2 (E of Zaragoza city, Tables 2 and 3). Both zones have Cl-SO_4-Na-Ca waters
220 with pH values mostly between 6.7 and 8.5. As a general trend, the highest pH values
221 are those from the irrigation waters, which also display the lowest alkalinity values and
222 electric conductivities. The electric conductivity values of the waters sampled in the
223 upstream Zone 1 are generally lower than those obtained for the selected points in Zone
224 2.

225 (insert here Tables 2 and 3)

226 Seasonal variations in the observed hydrochemistry can be assessed by examining the
227 data from each given point in the 2011-2012 campaigns (Table EA1 in the electronic

228 annex). According to the observed seasonal variations and groundwater types, three
229 groups of sampling points can be differentiated:

230 1) Roughly constant hydrochemistry throughout the year, with variations generally
231 smaller than 10% for most of the dissolved concentrations: this behavior is observed
232 for the sampling points 1WA2, 2SA1 and 2SA2 (Fig. 3a and Table EA1 in the
233 electronic annex). The sampling point 2WA7 could also be included in this group,
234 although its dissolved concentrations increase slightly (less than 15%) at the end of
235 the year. This group seems to correspond to sampling points influenced by a fairly
236 constant interaction with the evaporitic groundwater. This is apparent not only for the
237 wells 1WA2 and 2WA7, withdrawing groundwater from the evaporitic aquifer, but
238 also for the sinkhole ponds 2SA1 and 2SA2, in the light of their large and roughly
239 constant TDS values (generally above 1900 $mg \cdot L^{-1}$, larger than the average values
240 for the area; Table 3 and Table EA1 in the electronic annex).
241 2) Lowest dissolved concentrations for most of the elements between March and
242 July, in coincidence with the first months of the irrigation period. This trend is
243 mainly observed for the sinkholes 1HB1, 1HB2 and 1HB3 from Zone 1 (Fig. 3b and
244 Table EA1 in the electronic annex), although the evolution of the sinkhole 1HB2
245 could also been included in the previous group with small hydrochemical variations.
246 The observed hydrochemistry at those points is fairly dilute but more concentrated
247 than the corresponding irrigation waters in this zone, with average TDS below 600
248 mg/L (1IR3; Table 2). These characteristics suggest that the hydrochemistry in these
249 points is mainly determined by the features of the alluvial/irrigation waters, but with
250 some influence of mixing with groundwater from the underlying evaporitic aquifer
251 and/or of geochemical processes.

252 3) Lowest dissolved concentrations at the beginning of the year (January 2011),
253 strongly increasing thereafter to their maximum during the months with irrigation
254 (between April and October). This trend is observed for the sampling points 1WA3,
255 1WA4 and 2HA1, whose waters are fairly concentrated and display a wide range of
256 seasonal variability (Fig. 3c and Table EA1 in the electronic annex). These features
257 point towards the existence of variable interactions between the alluvial and the
258 evaporitic aquifer throughout the year, which will be explored further in the
259 following sections with the assistance of ion-ion plots and geochemical calculations.

260 (insert here Figure 3)

261 **4.2- Description of the main geochemical and hydrogeological processes**

262 The aim of this section is to detail the main identified geochemical and hydrogeological
263 processes potentially controlling the behavior of the Ebro alluvial-evaporitic karst
264 system. These processes were already described as a complement to exploratory
265 analyses using multivariate statistical techniques for the same area (see Acero *et al.*,
266 2013 for further details). However, this information is a key previous step for the
267 selection of processes to be included in the conceptual model for numerical calculations
268 and geochemical modeling. Therefore, the main processes identified in Acero *et al.*
269 (2013), will be shortly described below in order to facilitate the understanding of the
270 modeling sections and their results. Such geochemical and hydrogeological processes
271 are:

272 1- Halite and gypsum/anhydrite dissolution: the presence of minerals has been reported
273 for the studied area and the influence of their dissolution can be interpreted from the
274 correlations displayed by the molar dissolved concentrations of Na-Cl and Ca-SO_4
275 (Pearson correlation coefficients of 0.99 and 0.98, respectively; Table 4, and Fig. 4a,b

276 and c). As displayed in Fig. 5a, all the sampled waters are far from equilibrium with
277 respect to halite but some of the most concentrated samples from different wells and
278 springs are already equilibrated (within uncertainty) with respect to gypsum (Fig. 5b).
279 The Na/Cl stoichiometric ratios generally close to 1 (Tables 2 and 3) suggest that other
280 processes potentially affecting Na concentrations and that ratio, such as Na-exchange or
281 glauberite dissolution, have a minor contribution to the observed general
282 hydrochemistry.

283 (insert here Table 4, Figure 4 and Figure 5)

284 2- Mixing processes: the existence of mixing processes between the groundwater from
285 the alluvial and evaporitic materials seems evident after the examination of the Na-Cl
286 ion plot (Fig. 4a and b). Since halite is only present (in significant amounts) in the
287 evaporitic materials, the existence of large and well-correlated Na and Cl concentrations
288 in the groundwater from ponds and wells associated with the alluvial deposits can only
289 be explained as derived from the input of evaporitic groundwater. Consistent with this
290 explanation, the composition of most of the studied waters is linearly distributed in the
291 Na-Cl plot between the position of two types of end members: 1) irrigation waters (stars
292 in Fig. 4a and b), and 2) groundwater associated with the evaporitic aquifer (sampling
293 points 1WA2 and 2WA7; Fig. 4a and b).

294 3- Input and degassing of $CO_2(g)$: the presence of $CO_2(g)$ input probably derived from
295 biological activity in soils can be deduced from the calculated $CO_2(g)$ partial pressures
296 in equilibrium with many of the sampled waters (Fig. 5c), which are clearly larger than
297 the atmospheric value (i.e. around $10^{-3.5}$ atm). $CO_2(g)$ degassing seems to be especially
298 relevant for the aerated samples from irrigation waters and ponds (Fig. 5c), in contact
299 with atmospheric conditions and displaying $pCO_2(g)$ values closer to the atmospheric
300 ones.

4- Dissolution of carbonate minerals (calcite and dolomite) and possible precipitation of calcite. The presence of these mineral phases has been reported for both the alluvial and the evaporitic materials and, in the case of dolomite, this phase seems to be the main Mg mineral (Alberto and Navas, 1987; Salvany *et al*., 2007). Most of the sampled waters are either in equilibrium or oversaturated with respect to both calcite and dolomite, although oversaturation occurs mainly in surface waters with $pCO_2(g)$ close to equilibrium with atmospheric conditions (irrigation waters and ponds; stars, squares and rhombi in Fig. 5c), where it may be attributed to the already described $CO_2(g)$ degassing.

5- Other minor processes: the dissolution of aluminosilicate minerals seems also to take place in the system and mainly in the evaporitic materials, which would explain the positive correlation between Si concentrations and the concentrations of Ca, Mg, Sr and sulfate (with Pearson correlation coefficients between 0.57-0.72; Table 4). Finally, other processes (e.g. cation exchange or agricultural practices) may also occur in the system. Although their importance seems to be minor compared to the rest of processes already described, they could affect, for instance, the behavior of K and explain the lack of correlation between its concentrations and the concentrations of the rest of analyzed ions (Table 4).

4.3- Mass-balance calculations: conceptual model and general assumptions

Once the possible processes and factors controlling the observed hydrochemistry have been identified, their relative influence and seasonal variations at each sampling point have been assessed with the assistance of inverse (mixing + mass-balance) and forward (reaction-path) calculations (Zhu and Anderson, 2002). These calculations have been carried out only for the points specifically sampled for this study (detailed in Table 1), for which complete hydrochemical data throughout the hydrological year are available.

For the mixing + mass-balance calculations, the following hypotheses and procedures have been adopted:

- The observed major element hydrochemistry can be attributed to mixing of groundwater from the alluvial aquifer and the evaporitic aquifer and/or to geochemical processes. Thus, for each sample, the calculations were intended to reproduce the hydrogeochemical features of each sample as a mixture of certain proportions of groundwater from the alluvial and the evaporitic aquifer plus one or several reactions.
- The set of reactions included, in accordance with the described mineralogical composition for the Zaragoza Fm. and with the processes described in the previous section, is the following: (1) input or degassing of CO_2(g) and (2) dissolution or precipitation of calcite and gypsum and dissolution of dolomite and halite. Although the minor influence of other processes is also possible (e.g. influence of cation exchange), their associated uncertainties are so large that the resulting models would be highly speculative and unnecessarily complex (for the goals of the study). Thus, they have not been included in the assessed conceptual models.
- The groundwater composition in the evaporitic aquifer is estimated according to the hydrochemistry of samples that are clearly associated with the evaporitic materials (i.e. deep pumping wells with concentrated waters equilibrated with respect to gypsum; Fig. 5b). These samples are 1WA2-4, 1WA3-2 and 1WA4-3 for Zone 1 and 2WA7-2 for Zone 2. The hydrochemistry of these samples is detailed in Table 5.
- The dilute end-member in the alluvial aquifer is represented by the irrigation waters from each zone (irrigation is responsible for more than 90% of the recharge in the studied area; Durán *et al*., 2005); 1IR3 for Zone 1 (Table 3) and 2IR1 or 2IR2 for Zone 2 (Table 3). For each modeling case, the composition of the corresponding

irrigation water in a similar date has been selected as a proxy of the waters recharging the alluvial aquifer.

- In the case that different inverse models (mixing + reactions) are inferred for explaining the observed hydrochemistry at any given sampling point, the selection of the most feasible model was based on the following criteria: (1) thermodynamic feasibility of the resulting mass transferences (i.e. for each mineral phase, only undersaturated solutions are allowed to dissolve, and precipitation can only take place in oversaturated solutions), (2) minimum number of heterogeneous reactions involved, (3) consistency of the model with the ones inferred for other samples from the same sampling point (i.e. similar general models are preferred for explaining the whole set of hydrochemical observations at each sampling point).
- The analytical data for potassium, silica and strontium were not included in the model, since they are minor elements in the studied system and they are more affected by uncertainties regarding their possible geochemical controls (e.g. cation exchange, aluminosilicate dissolution, etc). For Sr, the observed concentrations and evolution can be reasonably attributed to the dissolution of gypsum or anhydrite, in whose lattice this element would appear (Kushnir, 1980; Lu *et al*., 1997). This can be deduced from: 1) the strong correlation of Sr concentrations with both sulfate and Ca concentrations, with Pearson correlation coefficients of around 0.9 (Table 4), and 2) fairly constant Sr:Ca molar ratios around 0.007 for both sampled zones (not shown).
- Owing to the uncertainties and simplifications related to the sample compositions used as representative for the alluvial/irrigation and evaporitic waters, the obtained results (i.e. mixing proportions, amounts of dissolved/precipitated phases) should only be interpreted as general trends rather than fixed values.

Prior to calculations, measured pH values have been corrected to account for the deviations caused at sampling points by CO_2(g) degassing due to extensive aeration by

contact with atmospheric conditions or even during sampling. As already explained, this process seems to be responsible for the apparent oversaturation with respect to calcite deduced for most of the surface waters. In order to correct this deviation, pH values in all the samples have been corrected in the subsequent calculations by imposing for each of them the pCO_2 necessary to attain calcite equilibrium, without any other changes in their hydrochemistry.

In order to check the suitability of the obtained inverse models (i.e. mixing proportions and geochemical reactions), they were tested by reaction-path calculations. In these calculations, the proportions of waters from the evaporitic and alluvial/irrigation proxies deduced for each sample were mixed and the calculated amounts of dissolved/precipitated/degassed phases were subsequently incorporated/substracted from the water compositions after mixing. The hydrochemical features obtained by means of the described reaction-path simulations were reasonably similar to the measured data in all the samples, being pH differences generally within ±0.06 pH units and absolute differences in the rest of dissolved concentrations mostly below 15% and frequently below 5%. These differences are considered acceptable taking into account the analytical and sampling errors and the uncertainties associated with the selection of the evaporitic and aquifer/irrigation proxies for each modeling case. Therefore, the results from reaction-path calculations fully support the conceptual models obtained by mixing + mass balance modeling presented in the following sections.

4.3.1- Results from mass-balance calculations for Zone 1

For the three ponds sampled at Zone 1 (1HB1, 1HB2 and 1HB3), the results suggest a mixture of minor amounts of groundwater from the evaporitic aquifer (5-30%, depending on the pond, sampling date and considered composition for the evaporitic waters) with the alluvial aquifer and/or irrigation waters, plus dissolution of $CO_2(g)$,

dolomite and halite, and occasional calcite dissolution or precipitation (see as an example the results for the pond 1HB1 in Fig. 6a). Roughly similar results (mixing and heterogeneous reactions) are obtained by using the composition of 1WA2-4, 1WA3-2 or 1WA4-3 (not shown) as representative from the hydrochemistry of the evaporitic aquifer.

All these reactions may be easily justified to occur in the alluvial materials during or after mixing except in the case of halite dissolution, whose presence in the alluvial materials is scarce. A possible explanation for the halite dissolution obtained with the calculations would be that this process takes place in the evaporitic materials before mixing with the alluvial groundwater. This would imply that the actual evaporitic groundwater mixing with the alluvial groundwater should have larger average Na and Cl concentrations than the 1WA2-4 sample used in the calculations.

In order to test this possibility, two additional sets of mass-balance calculations were performed using the composition of the 1WA2-4 sample as representative from the hydrochemistry of the evaporitic groundwater but increasing 4 and 7 times its Na and Cl dissolved concentrations, respectively (synthetic sample compositions 1WA2-MOD1 and 1WA2-MOD2; Table 5 and Fig. 4a). Those increase factors were chosen to make the Na and Cl concentrations in the 1WA2 sample roughly similar to the ones measured in other chosen evaporitic representatives richer in those elements and included in the modeling exercises (samples 1WA4-3 and 2WA7-2; Table 5). With these calculations, general mixing + reaction models similar to the one explained above, but without any halite dissolution, were obtained for almost all the samples from these three ponds (see representative examples using the composition of the 1WA2-MOD2 synthetic sample in Fig. 6b, c and d). Even though the calculated proportions of evaporitic groundwater decrease when increasing the Na and Cl concentrations in these waters, the obtained

427 evolution trends of mixing proportions and heterogeneous reactions throughout the year
428 are very similar for both sets of calculations.

429 (insert here Table 5 and Figure 6)

430 Therefore, the modeling results support the feasibility of this conceptual model to
431 explain the hydrochemical observations at the three ponds 1HB1, 1HB2 and 1HB3,
432 being at the same time consistent with the available mineralogical information (e.g.
433 halite present only in small amounts in the alluvial materials). Only two groups of
434 processes are necessary to justify the observations: 1) mixing between alluvial/irrigation
435 waters and evaporitic groundwater richer in Na and Cl than the one sampled at the
436 1WA2 well, and 2) dissolution of CO_2(g) and dolomite, and occasional calcite
437 dissolution or precipitation. However, an evaporitic end member richer in Na and Cl
438 than the sampled evaporitic groundwater is required in these calculations. Although the
439 existence of such hydrochemistry seems probable in the light of the larger Na and Cl
440 concentrations found in other wells withdrawing water from the evaporitic materials
441 (wells 1WA4-3 and 2WA7; Table 5), additional deep wells in Zone 1 would be
442 necessary in order to fully confirm this hypothesis.

443 According to this conceptual model, the calculated mixing proportions for the sinkhole
444 pond 1HB1 seem to range between 70-80% and 90-95% of alluvial water throughout
445 the year (Fig. 6b). A sharp increase in the contribution of these waters is observed in
446 coincidence with the beginning of the irrigation season in the area (March-April 2011).
447 This large contribution of around 90% of alluvial/irrigation waters is maintained during
448 the whole irrigation period (until October 2011), decreasing thereafter to similar values
449 to the ones calculated for the period preceding the irrigation season (Fig. 6b). For the
450 ponds 1HB2 and 1HB3, similar mixing proportions are obtained, with more than 80%
451 of alluvial/irrigation water contribution throughout the year (Fig. 6c and d). As a general

452 trend, a slight decrease in the relative contribution of evaporitic groundwater is
453 calculated for the months corresponding to the irrigation season (between March and
454 October), which is consistent with the expected hydrogeological regime of the system.

455 For the pumping wells 1WA3 and 1WA4, the hydrochemistry of the evaporitic
456 groundwater has been represented by the composition of the samples 1WA3-2 and
457 1WA4-3, respectively (Table 5). These samples have been selected as evaporitic end
458 members for these wells because they display the highest dissolved concentrations for
459 most of the elements (Table EA1 in the electronic annex) and they are close to
460 equilibrium with respect to gypsum (Fig. 5b). These features support their probable
461 association with the evaporitic materials and their local representativeness of the
462 variable hydrochemistry of evaporitic groundwater. For these two wells, the inferred
463 geochemical processes are mainly CO_2(g) input, dolomite dissolution and calcite
464 dissolution/precipitation (Fig. 6e and f). Regarding the proportions of mixing waters,
465 the deduced contribution of evaporitic groundwater is larger (generally above 40%; Fig.
466 6e and f) than in the previously described ponds, which is consistent with the fact that
467 both wells reach the evaporitic bedrock (Table 1). Evaporitic groundwater proportions
468 increase during the irrigation period up to 80-100% (Fig. 6e and f), which could be
469 attributed to their upwelling associated with pumping for irrigation purposes during that
470 period. An important implication of the observed behaviour is the possibility that
471 pumping leads to high local hydraulic gradients within the alluvial and evaporitic
472 materials and to a decline in the water table (depression cones). These changes may
473 favour mineral dissolution (due to the increase of water flow rates) and the loss of
474 buoyant support. Both effects are relevant, since they might accelerate the subsidence
475 on existing sinkholes or even create new ones (Gutiérrez et al., 2008b). In fact, the well

476 1WA3 is located within a damaging sinkhole with estimated subsidence rates of 7 cm/yr
477 (Galve et al., 2009).

478 **4.3.2- Results from mass-balance calculations for Zone 2**

479 In the mass-balance calculations carried out for this zone, the hydrochemistry of the
480 alluvial/irrigation waters was represented by the composition of IR1 for the sampling
481 points 2SA2 and 2HA1, and IR2, for the 2SA1 spring. This selection was based on the
482 proximity of the sampling points to the Urdana ditch or to the Ebro River (Fig. 1). The
483 hydrochemistry of the evaporitic aquifer was represented by the composition of the
484 groundwater sampled in the pumping well 2WA7, drilled directly in the evaporitic
485 bedrock on the northern valley margin and whose hydrochemistry corresponds clearly
486 to these materials (Tables 1 and 5). In order to consider for this evaporitic groundwater
487 a composition representative for the largest possible time span of the year, the
488 hydrochemistry of sample 2WA7-2 was selected (Table 5).

489 As displayed in Fig. 7 and also described for Zone 1, mixing between evaporitic and
490 alluvial/irrigation waters plus some geochemical reactions can account for the observed
491 hydrochemistry at the three sampling points of Zone 2 throughout the year. With regard
492 to the calculated geochemical processes, CO_2(g) input to the groundwater and, in some
493 cases, some gypsum, calcite, dolomite and, especially, halite dissolution is required to
494 account for the observed hydrochemistry (see a representative example for the sampling
495 point 2SA2 in Fig. 7a). All these processes can be justified in the alluvial materials
496 based on their reported mineralogy except halite dissolution, which must mainly take
497 place in the evaporitic materials. Analogously to Zone 1, larger sodium and chloride
498 concentrations would be necessary in the evaporitic groundwater contributing to mixing
499 than the ones sampled at the well 2WA7.

500 (insert here Figure 7)

501 In fact, when sodium and chloride concentrations in the evaporitic end-member are
502 doubled (composition 2WA7-MOD, from now on; Table 5 and Fig. 4b), halite
503 dissolution is not required to reproduce the observations at any of the target sampling
504 points (Fig. 7b, c and d), being the rest of the results notably similar (see a
505 representative comparison of results for the sampling point 2SA2 in Fig. 7a and b). For
506 simplicity, the composition 2WA7-MOD will be assumed as the evaporitic end member
507 for Zone 2 in the description of results detailed below. However, similar results have
508 been obtained using the originally sampled 2WA7-2 composition but in that case
509 including some halite dissolution, as shown for the sampling point 2SA2 (Fig. 7a and
510 b).

511 For the spring 2SA1, located in the floodplain, the calculations suggest that the
512 contribution of evaporitic groundwater is minor (between 9 and 16%) and fairly
513 constant throughout the year (Fig. 7c). A slight decrease in the relative contribution of
514 groundwater from the evaporitic aquifer is inferred after April 2011 and towards the end
515 of the year, which could be attributed to the impact of irrigation during this period.
516 Apart from mixing, dissolution of CO_2(g) and minor amounts of dolomite (always less
517 than 130 mg/L) are also suggested by the model results.

518 Regarding the spring 2SA2, the deduced proportions of evaporitic groundwater
519 contributing to the observed hydrochemistry are generally much higher than at spring
520 2SA1, ranging roughly between 30 and 50% throughout the year (Fig. 7a and b). The
521 contribution of the evaporitic aquifer seems to be highest in April 2011 and decreases
522 thereafter towards January 2012, as also described for the spring 2SA1, most probably
523 due to similar reasons. Only some extra CO_2(g) and calcite dissolution, in addition to
524 mixing, are required to explain the measured hydrochemistry and its temporal
525 variability.

526 Similarly, the hydrochemical evolution at the 2HA1 sinkhole pond can also be
527 explained by mixing plus some CO_2(g) input, with dolomite, calcite and gypsum
528 dissolution only for some months (Fig. 7d). Surprisingly, the proportion of evaporitic
529 groundwater contributing to the hydrochemistry at this sinkhole pond seems to increase
530 from around 10% to 21-25% during the irrigation season (from March 2011; Fig. 7d). If
531 this mixing model is accepted, this result would imply the rise of evaporitic waters
532 during this period. Although the lack of detailed hydrogeological information from the
533 area prevents from obtaining any unequivocal interpretation for this behavior, a possible
534 cause for such groundwater rise could be the presence of a lateral facies change from
535 evaporitic materials to impervious clays just downstream of this sampling point (Fig.
536 1b). This change from karstified to impervious bedrock might act as a hydrogeological
537 barrier, forcing the rise of deep and highly saline flows from the evaporitic aquifer,
538 creating a zone of focused upward discharge.

539 An alternative explanation to the observed increase of most dissolved concentrations at
540 the sampling point 2HA1 during the irrigation season could be the possible presence of
541 high soil salinity associated with the high evapotranspiration and shallow water head
542 levels (at around 2-4 meters depth). This would imply the existence of active mineral
543 precipitation linked to evapotranspiration in the vadose zone, followed by re-dissolution
544 of those mineral phases and transport of the dissolved elements towards the
545 groundwater linked to irrigation. The results obtained in mass-balance calculations
546 using this alternative conceptual model (i.e. alluvial/irrigation waters + reactions) for
547 the 2HA1 point are displayed in Fig. 7e, showing that the main dissolved phases in the
548 vadose zone would be gypsum and, especially, halite.

549 In order to confirm or discard these hypotheses, new studies focused on the evolution of
550 salinity in soil profiles throughout the year and on the hydrogeological processes in the
551 surroundings of the 2HA1 should be carried out in the future.

552 **5- SUMMARY AND CONCLUSIONS**

553 The application of geochemical modelling to the quantification of hydrogeological and
554 geochemical processes in the studied stretch of the Ebro Valley (NE Spain) has
555 provided new insights on the behaviour of this system affected by evaporite
556 karstification at a relatively low cost.

557 The hydrogeology and hydrochemistry of the system may be explained by the mixing of
558 groundwater from the evaporitic aquifer and the overlying alluvial aquifer. Such mixing
559 controls the wide range of water compositions observed in different sinkhole ponds,
560 springs and pumping wells. For the sinkhole ponds, the proportion of evaporitic
561 groundwater required to justify the observed hydrochemistry varies between 5 and 50%
562 of the water volume in the pond. The effects of pumping and irrigation seem to play a
563 key role in the seasonal evolution of mixing proportions of groundwater from the
564 evaporitic and the alluvial aquifer.

565 According to the obtained results, the following hydrogeological conclusions can also
566 be obtained:

567 - There is a good connection between the evaporite karst and the alluvial aquifers, as
568 suggested by: 1) the rapid response of the karst aquifer hydrochemistry to recharge by
569 irrigation, and 2) the deduced input of evaporitic groundwater in all the studied ponds.

570 - Different hydrogeological features and processes are observed in various parts of the
571 alluvial/evaporitic aquifer system, as suggested mainly by the different hydrochemical
572 response to irrigation. These variations can be grouped in three main trends: 1) dilute

573 alluvial waters receiving a small influence of groundwater from the evaporitic aquifer,
574 especially during the irrigation campaigns (e.g. ponds 1HB1 and 1HB2; Fig. 8); 2)
575 concentrated waters affected by the rise of evaporite groundwater owing to pumping
576 during the irrigation campaigns (e.g. wells 1WA3 and 1WA4; Fig. 8) or to other
577 processes (sinkhole pond 2HA1; Fig. 8); 3) saline waters associated with the evaporitic
578 aquifer and roughly unaffected by irrigation (sampling wells 1WA2 and 2WA7; Fig. 8).

579 (insert here Figure 8)

580 Apart from the described hydrogeological controls, the hydrogeochemical behaviour of
581 the study area is influenced by the following geochemical processes, in order of
582 decreasing relative importance: (1) dissolution of gypsum and halite, mainly in the
583 evaporitic aquifer; (2) CO_2(g) dissolution, probably associated with the percolation of
584 alluvial/irrigation waters through soils with active biological processes; and (3)
585 dissolution of dolomite and calcite dissolution/precipitation, both in the alluvium and in
586 the evaporitic bedrock.

587 Whereas the groundwater circulating through the evaporitic bedrock seems to have
588 reached equilibrium with respect to gypsum, it is far from equilibrium with respect to
589 halite. Therefore, active subsidence associated with halite dissolution is expected to
590 continue until halite becomes exhausted. Since irrigation waters are very undersaturated
591 with respect to gypsum, an episodic increase of gypsum dissolution associated with
592 their input is expected, which may also contribute to subsidence phenomena. The
593 presence of these active dissolution processes suggests that there is a clear potential of
594 future subsidence due to further karstification in the area.

595 In general, the results of this study show the applicability of the used methodology to
596 explore the hydrogeological and geochemical processes in areas with scarce direct
597 information. Although a more detailed hydrogeological, hydrochemical and

598 mineralogical characterization of the studied portion of the Ebro Valley should be
599 carried out in the future, the proposed conceptual model represents a helpful step
600 towards the understanding and management of the subsidence hazard in this area.

601

6- ACKNOWLEDGEMENTS

The authors wish to thank the Ebro Water Authority (CHE) for giving access to hydrochemical and other data used in this study. We would like to thank particularly the gentle help and support from Dr. Miguel Ángel García Vera, Felipe Delgado, Teresa Carceller and Vicente Sancho-Tello. We thank Dr. Pedro Lucha, who assisted with the fieldwork and made interesting contributions in the first steps of the project. We also thank Mr. José Ángel Navamuel (Zaragoza Municipality) for helping us to obtain permits to sample water from wells. The assistance of Enrique Oliver with some of the analytical determinations is also gratefully acknowledged. EBRONAUTAS SLL has handed over the cataraft used in the sampling survey. Authors would like to acknowledge the use of Servicio General de Apoyo a la Investigación-SAI, Universidad de Zaragoza. Dr. Acero and Dr. Asta have received economical support from the Spanish Ministry of Science and Innovation through Research Contracts from the "Juan de la Cierva Subprogram". The economic support of the European Social Fund and of the Aragon Government (DGA) through their program for financing research in Consolidated Groups is also acknowledged. The investigation has been also partially financed by the projects CGL2010-16775 (Ministerio de Ciencia e Innovación and FEDER), 2012/GA-LC-021 (Gobierno de Aragón-La Caixa) and CGL2013-40867-P (Ministerio de Economía y Competitividad).

622 **7- REFERENCES**

623 Acero, P., Gutiérrez, F., Galve, J. P., Auqué, L. F., Carbonel, D., Gimeno, M. J. Gómez,
624 J. B., Asta, M.P. and Yechieli, Y. 2013. Hydrogeochemical characterization of an
625 evaporite karst area affected by sinkholes (Ebro Valley, NE Spain). Geologica
626 Acta 11(4), 389-407.

627 Alberto, F., Navas, A. 1987. Characterization of calcite, dolomite and gypsum
628 saturation levels in the surface waters of the Ebro river basin. An. Aula Dei 18 (3-
629 4), 199-228.

630 Apaydin, A., Aktas, S.D., 2012. Assessment of groundwater quality of the Tatlicay
631 aquifer and relation to the adjacent evaporitic formations (Cankiri, Turkey).
632 Environ. Monit, Assess., 184, 2337–2357.

633 Aquilina, L., Ladouche, B., Doerfliger, N., Bakalowicz, M., 2003. Deep water
634 circulation residence time and chemistry in a karst complex. Ground Water, 41
635 (6), 790–805.

636 Aquilina, L., Ladouche, B., Doerfliger, N., 2005. Recharge processes in karstic systems
637 investigated through the correlation of chemical and isotopic composition of rain
638 and spring-waters. Appl. Geochem., 20, 2189–2206.

639 Aquilina, L., Ladouche, B., Doerfliger, N. 2006. Water storage and transfer in the
640 epikarst of karstic systems during high flow periods. J. Hydrol., 327(3-4), 472-
641 485.

642 Auqué, L.F., Acero, P., Gimeno, M.J., Gomez, J.B., Asta, M.P., 2009.
643 Hydrogeochemical modeling of a thermal system and lessons learned for CO_2
644 geologic storage. Chem. Geol., 268, 324–336.

645 Ball J.W., Nordstrom, D.K, 2001. User's manual for WATEQ4F, with revised
646 thermodynamic data base and test cases for calculating speciation of major, trace,
647 and redox elements in natural waters. US Geological Survey Open File Report 91-
648 183, USA.

649 Barbieri, M., Boschetti, T., Petitta, M., Tallini, M., 2005. Stable isotope (H-2, O-18 and
650 Sr-87/Sr-86) and hydrochemistry monitoring for groundwater hydrodynamics
651 analysis in a karst aquifer (Gran Sasso, Central Italy). Appl. Geochem., 20, 2063–
652 2081.

653 Barberá, J.A., Andreo, B., 2012. Functioning of a karst aquifer from S Spain under
654 highly variable climate conditions, deduced from hydrochemical records. Environ.
655 Earth Sci., 65, 2337–2349.

656 Belkhiri, L., Boudoukha, A., Mouni, L. Baouz, T. 2010. Application of multivariate
657 statistical methods and inverse geochemical modeling for characterization of
658 groundwater. A case study: Ain Azel plain (Algeria). Geoderma, 159; 390-398.

659 Bicalho, C.C., Batiot-Guilhe, C., Seidel, J.L., Van Exter, S., Jourde, H., 2012.
660 Geochemical evidence of water source characterization and hydrodynamic
661 responses in a karst aquifer. J. Hydrol., 450-451, 206–218.

662 Castañeda C., Gutiérrez F., Manunta M., Galve J.P., 2009. DInSAR measurements of
663 ground deformation by sinkholes, mining subsidence, and landslides, Ebro River,
664 Spain. Earth Surface Processes and Landforms 34 (11), 1562–1574.

665 Carucci, V., Petitta, M., Aravena, R., 2012. Interaction between shallow and deep
666 aquifers in the Tivoli Plain (Central Italy) enhanced by groundwater extraction: A
667 multi-isotope approach and geochemical modeling. Appl. Geochem., 27, 266–
668 280.

669 Chiesi, M., Waele, J. D., Paolo, F., 2010. Origin and evolution of a salty
670 gypsum/anhydrite karst spring: The case of Poiano (Northern Apennines, Italy).
671 Hydrogeol. J., 18, 1111–1124.

672 Dassi, L., 2011. Investigation by multivariate analysis of groundwater composition in a
673 multilayer aquifer system from North Africa: A multi-tracer approach. Appl.
674 Geochem., 26, 1386–1398.

675 Diputación General de Aragón, 2007. Atlas climático de Aragón. Gobierno de Aragón,
676 Departamento de medio ambiente, 222pp. Available at: http://www.aragon.es/
677 DepartamentosOrganismosPublicos/Departamentos/AgriculturaGanaderiaMedioA
678 mbiente/AreasTematicas/MA_CambioClimatico/EACCEL/LineasActuacionProye
679 cto/ci.07_01_Atlas_Climatico_Aragon.detalleDepartamento).

680 Durán J., Garrido E., García M., 2005. Informe: Trabajos técnicos para la aplicación de
681 la Directiva Marco del Agua en materia de Aguas Subterráneas. Caracterización
682 Adicional Aluvial del Ebro-Zaragoza. Instituto Geológico y Minero de España.
683 Dirección General del Agua. 112 pp.

684 Fidelibus, M.D., Gutiérrez, F., Spilotro, G., 2011. Human-induced hydrogeological
685 changes and sinkholes in the coastal gypsum karst of Lesina Marina area (Foggia
686 Province, Italy). Eng. Geol., 118, 1-19.

687 Galve, J.P., Gutiérrez, F., Lucha, P., Bonachea, J., Cendrero, A., Gimeno, M.J.,
688 Gutiérrez, M., Pardo, G., Remondo, J., Sánchez, J.A., 2009. Sinkholes in the salt-
689 bearing evaporite karst of the Ebro River valley upstream of Zaragoza city (NE
690 Spain). Geomorphological mapping and analysis as a basis for risk management.
691 Geomorphology, 108, 145-158.

692 Günay, G., 2002. Gypsum karst, Sivas, Turkey. Environ. Geol., 42, 387–398.

693 Guerrero, J., Gutiérrez, F., Lucha, P., 2008a. The impact of halite dissolution
694 subsidence on fluvial terrace development. The case study of the Huerva River in
695 the Ebro Basin (NE Spain). Geomorphology, 100, 1-2, 164-179.

696 Guerrero, J., Gutiérrez, F., Bonachea, J., Lucha, P., 2008b. A sinkhole susceptibility
697 zonation based on paleokarst analysis along a stretch of the Madrid-Barcelona
698 high-speed railway built over gypsum- and salt-bearing evaporites (NE Spain).
699 Eng. Geol., 102, 62-73.

700 Guerrero, J., Gutiérrez, F., Galve, J.P., 2013. Large depressions, thickened terraces and
701 gravitational deformation in the Ebro River valley (Zaragoza area, NE Spain).
702 Evidence of glauberite and halite interstratal karstification. Geomorphology, 196,
703 162-176.

704 Gutiérrez, F., Galve, J.P., Guerrero, J., Lucha, P., Cendrero, A., Remondo, J., Bonachea,
705 J., Gutiérrez, M., Sánchez, J.A. (2007). The origin, typology, spatial distribution,
706 and detrimental effects of the sinkholes developed in the alluvial evaporite karst
707 of the Ebro River valley downstream Zaragoza city (NE Spain). Earth Surf.
708 Processes and Landforms, 32, 912-928.

709 Gutiérrez, F., Calaforra, J.M., Cardona, F., Ortı, F., Durán, J. J., Garay, P., 2008a.
710 Geological and environmental implications of the evaporite karst in Spain.
711 Environ. Geol., 53, 951–965.

712 Gutiérrez F., Johnson K.S., Cooper A.H., 2008b. Evaporite karst processes, landforms,
713 and environmental problems. Environmental Geology 53 (5), 935–936.

714 Gutiérrez, F. 2010. Hazards associated with karst. In: Alcántara, I. and Goudie, A.
715 (Eds.). Geomorphological Hazards and Disaster Prevention. Cambridge
716 University Press. Cambridge, 161-175.

717 Huang, P., Chen, J., 2012. Recharge sources and hydrogeochemical evolution of
718 groundwater in the coal-mining district of Jiaozuo, China. Hydrogeol. J., 20(4):
719 739–754.

720 Jiménez-Torrecilla, N., Galve, J.P., Asta, M.P., Gómez, L., Fuentes, J., 2004. Los
721 humedales salinos del entorno de Zaragoza: una singularidad
722 hidrogeomorfológica. GeoTemas (6), 115-118.

723 Kaçaroglu, F., Degirmenci, M., Cerit, O., 2001. Water quality problems of a
724 gypsiferious watershed: Upper Kizilirmak basin, Sivas, Turkey. Water, Air, Soil
725 Pollut., 128, 161–180.

726 Kushnir, J., 1980. The coprecipitation of strontium, magnesium, sodium, potassium and
727 chloride ions with gypsum. An experimental study. Geochim. Cosmochim. Acta,
728 44, 1471–1482.

729 Lamont-Black, J., Younger, P. L., Forth, R. A., Cooper, A. H., Bonniface, J. P., 2002. A
730 decision-logic framework for investigating subsidence problems potentially
731 attributable to gypsum karstification, Eng. Geol., 65, 205–215.

732 Lamont-Black, J., Baker, A., Younger P. L., Cooper, A.H., 2005. Utilising seasonal
733 variations in hydrogeochemistry and excitation-emission fluorescence to develop
734 a conceptual groundwater flow model with implications for subsidence hazards:
735 an example from Co. Durham, UK. Environ. Geol., 48, 320-335.

736 Land A.L., 2003. Evaporite karst and regional groundwater circulation in the Lower
737 Pecos Valley of Southeastern New México. In: Johnson K.H., Neal J.T. (eds.).
738 Evaporite karst and engineering/environmental problems in the United States.
739 Oklahoma Geological Survey Circular, 109, 227-232.

740 Langmuir, D., Melchior, D., 1985. The geochemistry of Ca, Sr, Ba and Ra sulfates in
741 some deep brines from the Palo Duro basin, Texas. Geochim. Cosmochim. Acta,
742 49, 2423–2432.

743 Lee E.S., Krothe N.C., 2001. A four-component mixing model for water in a karst
744 terrain in south-central Indiana, USA. Using solute concentration and stable
745 isotopes as tracers. Chem. Geol. 179:129–143

746 López-Chicano, M., Bouamama, M., Vallejos, A., Pulido-Bosch, A., 2001. Factors
747 which determine the hydrogeochemical behaviour of karstic springs. A case study
748 from the Betic Cordilleras, Spain. Appl. Geochem., 16, 1179-1192.

749 Lu, F.H., Meyers, W.J., Schoonen, M.A.A., 1997. Minor and trace element analyses on
750 gypsum: an experimental study. Chem. Geol. 142(1–2), 1-10.

751 Marković, T., Brkić, Ž., Larva, O. 2013. Using hydrochemical data and modelling to
752 enhance the knowledge of groundwater flow and quality in an alluvial aquifer of
753 Zagreb, Croatia. Science of the Total Environment, 458, 508-516.

754 Moore, P.J., Martin, J.B., Screaton, E.J., 2009. Geochemical and statistical evidence of
755 recharge, mixing, and controls on spring discharge in an eogenetic karst aquifer. J.
756 Hydrol., 376, 443–455.

757 Moral, F., Cruz-Sanjulián, J.J., Olías, M., 2008. Geochemical evolution of groundwater
758 in the carbonate aquifers of Sierra de Segura (Betic Cordillera, southern Spain). J.
759 Hydrol. 360 (1–4), 281–296.

760 Nemeth, K., 1963. Photometric determination of sulphate in soil extracts. Z. PflErnahr.
761 Dung. 103, 193–196.

762 Ninyerola, M., Pons, X., Roure, J.M, 2005. Atlas Climático Digital de la Península
763 Ibérica. Metodología y aplicaciones en bioclimatología y geobotánica.
764 Universidad Autónoma de Barcelona, Bellaterra. 44 pp.

765 Omelon, C.R., Pollard, W.H., Andersen, D.T., 2006. A geochemical evaluation of
766 perennial spring activity and associated mineral precipitates at Expedition Fjord,
767 Axel Heiberg Island, Canadian High Arctic. Appl. Geochem., 21, 1-15.

768 Ortí, F., Salvany, J.M., 1997. Continental evaporitic sedimentation in the Ebro Basin
769 during the Miocene. In: Busson, G., Schreiber, B.Ch. (eds.). Sedimentary
770 deposition in rift and foreland basins in France and Spain. Columbia University
771 Press, New York, 420-429.

772 Parkhurst, D.L., Appelo, C.A.J., 2013. Description of input and examples for
773 PHREEQC version 3—A computer program for speciation, batch-reaction, one-
774 dimensional transport, and inverse geochemical calculations: U.S. Geological
775 Survey Techniques and Methods, book 6, chap. A43, 497 p., available only at
776 http://pubs.usgs.gov/tm/06/a43/.

777 Plummer, N., Busby, J., Lee, R., Hanshaw, B., 1990. Geochemical modeling of the
778 Madison aquifer in parts of Montana, Wyoming and South Dakota. Water Resour.
779 Res., 26, 1981-2014.

780 Quirantes, J., 1978. Estudio sedimentológico y estratigráfico del Terciario continental
781 de los Monegros. Institución Fernando el Católico, CSIC, Zaragoza, 200 pp.

782 Sánchez, J. A., Jiménez, N., Galve, J.P., Asta, M.P., 2004. Estudio hidrogeológico de la
783 subsidencia y los humedales salinos en el entorno de Zaragoza. Unidad de Montes
784 y Áreas Naturales, Excmo. Ayuntamiento de Zaragoza, Zaragoza. Unpublished
785 Report.

786 Salvany J.M., García-Veigas, J., Ortí, F., 2007. Glauberite-halite association of the
787 Zaragoza Gypsum Formation (Lower Miocene, Ebro Basin, NE Spain).
788 Sedimentology, 54, 443–467.

789 Salvany J.M., 2009. Geología del yacimiento glauberítico de Montes de Torrero
790 (Zaragoza). Prensas Universitarias de Zaragoza, Zaragoza, 80 pp.

791 Salvati, R., Sasowsky, I.D., 2002. Development of collapse sinkholes in areas of
792 groundwater discharge. J. Hydrol., 264, 1–11.

793 Tuccimei, P., Salvati, R., Capelli, G, Delitala, M.C., Primavera, P., 2005. Groundwater
794 fluxes into a submerged sinkhole area, Central Italy, using radon and water
795 chemistry. Appl. Geochem., 20, 1831–1847.

796 Uliana, M.M, Sharp., J.M., 2001. Tracing regional flow paths to major springs in Trans-
797 Pecos Texas using geochemical data and geochemical models. Chem. Geol., 179
798 (1–4), 53-72.

799 Waltham, T., Bell, F., Culshaw, M., 2005. Sinkholes and subsidence. Springer,
800 Chichester, 382 pp.

801 Wang, Y., Ma, T., Luo, Z., 2001. Geostatistical and geochemical analysis of surface
802 water leakage into groundwater on a regional scale: a case study in the Liulin
803 karst system, northwestern China. J. Hydrol., 246, (1–4), 223-234.

804 Wong, C.I., Mahler, B.J., Musgrove, M., Banner, J.L., 2012. Changes in sources and
805 storage in a karst aquifer during a transition from drought to wet conditions. J.
806 Hydrol., 468–469, 159-172.

807 Xie, X., Wang, Y., Ellis, A., Su, C., Li, J., Li, M, Duan, M. 2013. Delineation of
808 groundwater flow paths using hydrochemical and strontium isotope composition:

809 A case study in high arsenic aquifer systems of the Datong basin, northern China.
810 J. Hydrol., 476, 87-96.

811 Yechieli, Y., Abelson, M., Bein, A., Crouvi, O., Shtivelman, V., 2006. Sinkhole
812 "swarms" along the Dead Sea coast: Reflection of disturbance of lake and
813 adjacent groundwater systems. Geological Society of America Bulletin, 118(9-
814 10), 1075-1087.

815 Zhu, C., Anderson, G. 2002. Environmental applications of geochemical modeling.
816 Cambridge University Press.

817

818 **FIGURE CAPTIONS**

819 Figure 1: a: Location and geological settings of the studied area and position of the
820 selected sampling points for hydrochemical characterisation. b: Schematic cross-
821 sections perpendicular (A-A') and roughly parallel (B-B') to the Ebro Valley, showing
822 the general distribution of the main lithostratigraphic units and the weathering zone in
823 which anhydrite and glauberite are replaced by secondary gypsum. These sections are
824 based on borehole data from the southern margin of the valley (Salvany, 2009) and
825 assume a roughly symmetric configuration at both sides of the valley, excavated along
826 the axial zone of a very gentle syncline.

827 Figure 2:a: Aerial view of the Ebro River valley upstream of Zaragoza city showing the
828 evaporitic bedrock (escarpment) and the valley bottom underlain by the alluvial aquifer;
829 b: Ojo del Fraile pond (ca. 240 m long) developed in a sagging sinkhole with nested
830 collapse dolines (sampling point 1HB1); c: Ojos de Matamala sinkhole ponds. The
831 subcircular lake, 30 m in diameter, corresponds to sampling point 2HA1. A maximum
832 depth of 3.5 m was measured in April 2009; d: Pond 55 m across in Torre del
833 Chocolatero collapse sinkhole (sampling point 1HB2). A maximum water depth of 6.6
834 m was measured in April 2009.

835 Figure 3: Variation trends of TDS concentrations in the sampled waters throughout the
836 year. Pannels a, b and c display the different trends for the three groups of sampling
837 points described in the text: a) group with roughly constant hydrochemistry throughout
838 the year; b) group with lowest dissolved contents at the beginning of the irrigation
839 season (March-July); and c) group with lowest dissolved contents at the beginning of
840 the year, increasing thereafter to their maximum during the months with irrigation
841 (April-October).

842 Figure 4: Correlation between some of the main hydrochemical parameters in the water
843 samples from the studied system. a and b: Chloride vs. sodium dissolved concentrations
844 in Zone 1 (a) and 2 (b). Be aware of the different scale for Cl concentrations between
845 both panels; c: Sulfate vs. calcium dissolved concentrations. The position corresponding
846 to the synthetic sample compositions used for representing the evaporitic groundwater
847 in the mass-balance calculations (1WA2-MOD1, 1WA2-MOD2 and 2WA7-MOD) is
848 also included in panels a and b. Modified and simplified from Acero *et al.* (2013).

849 Figure 5: Correlation between calculated saturation indexes and with some
850 hydrochemical parameters in the water samples from the studied system. a: Halite
851 saturation index vs. Total Dissolved Solids (TDS); b: Gypsum saturation index vs. TDS;
852 c: log[$pCO_2(g)$] vs Calcite saturation index; d: Dolomite saturation index vs. Calcite
853 saturation index. The uncertainty range for the saturation indexes of gypsum, calcite and
854 dolomite are 0.22 (Langmuir and Melchior, 1985**)**, 0.35 (Plummer *et al*., 1990**)** and 0.5
855 (Plummer *et al*., 1990), respectively. Modified and simplified from Acero *et al.* (2013).

856 Figure 6: Summary of results of some of the mixing + mass balance models for Zone 1
857 carried out in this study. a and b: results of models of mixing between irrigation/alluvial
858 waters and evaporitic waters + heterogeneous reactions for the pond 1HB1, using as
859 evaporitic end members the compositions of the sample 1WA2-4 and of the synthetic
860 sample 1WA2-MOD2 (see Fig. 4a and text for details), respectively; c and d; results of
861 the same type of models for the ponds 1HB2 and 1HB3, respectively, using as
862 evaporitic end member the composition of the synthetic sample 1WA2-MOD2; e and f:
863 results of the same type of models for the sampling points 1WA3 (e) and 1WA4 (f),
864 using as evaporitic end members the compositions of the samples 1WA3-2 and 1WA4-
865 3, respectively.

Figure 7: Summary of results of some of the mixing + mass balance models from Zone 2 carried out in this study: a and b: results of models of mixing between irrigation/alluvial waters and evaporitic waters + heterogeneous reactions for the spring 2SA2, using as evaporitic end members the compositions of the samples 2WA7-2 and 2WA7-MOD, respectively (see Fig. 4b and text for details); c and d: results of the same type of models for the spring 2SA1 (c) and the sinkhole pond 1HA1 (d), using as evaporitic end members the composition of the synthetic sample 2WA7-MOD; e: results of model without mixing for the sinkhole pond 2HA1.

Figure 8: Schematic 3D-block (not at scale) showing the main hydrogeological situations that have been inferred for the studied zones.

TABLE CAPTIONS

Table 1: General features of the sampling points included in this study. The codes for the sampling points consist of four numbers and capital letters: first, a number (1 or 2) indicates if the point is located W of the confluence between the Ebro and Gallego rivers (Zone 1), or to the E (Zone 2), respectively (Fig. 1); then, a capital letter indicates if the point corresponds to a well (-W--), a spring (-S--) or a pond (-H--), and a second letter is used to indicate if the water at that point can be considered as relatively concentrated (--A-) or diluted (--B-), compared to the average TDS of the study area, which is around 1600 mg/L according to our data. Additionally, IR points correspond to irrigation waters. Finally, consecutive numbers allow differentiating the different sampling points.

Table 2: Average hydrochemical features of the sampling points included in this study for Zone 1. Statistics for strontium and silica dissolved concentrations are not shown

889 because they are only available for some of the points (see Table EA1 in the electronic
890 annex).

891 Table 3: Average hydrochemical features of the sampling points included in this study
892 for Zone 2. Statistics for strontium and silica dissolved concentrations are not shown
893 because they are only available for some of the points (see Table EA1 in the electronic
894 annex).

895 Table 4: Pearson correlation coefficients between the different variables included in this
896 study, obtained from the whole available dataset (see Table EA1 in the electronic
897 annex).

898 Table 5: Hydrochemical features of the samples chosen as representative from the
899 evaporitic aquifer groundwater in the mixing + mass balance geochemical calculations.

900

Figure 1

Click here to download high resolution image

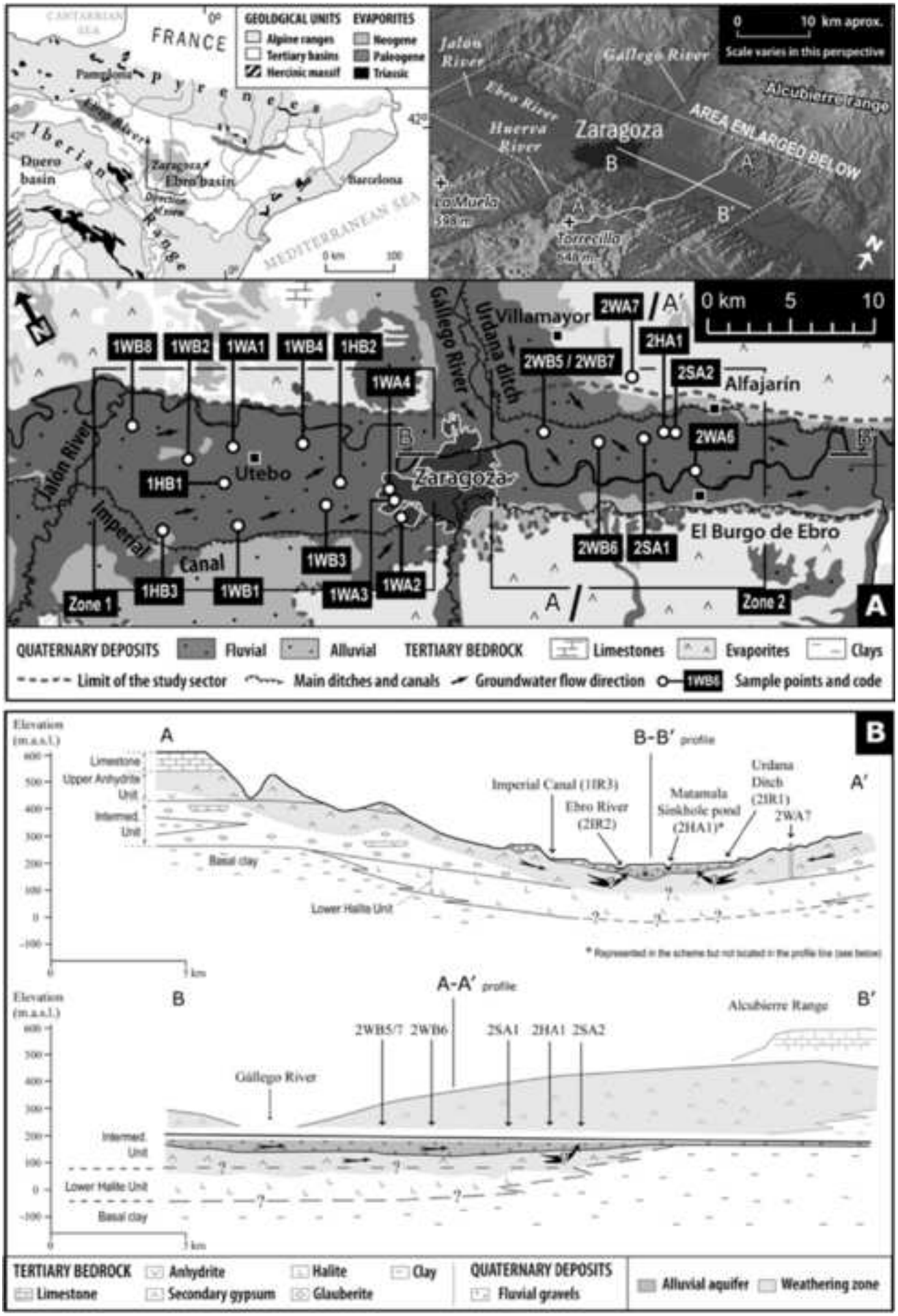

Figure 2

Click here to download high resolution image

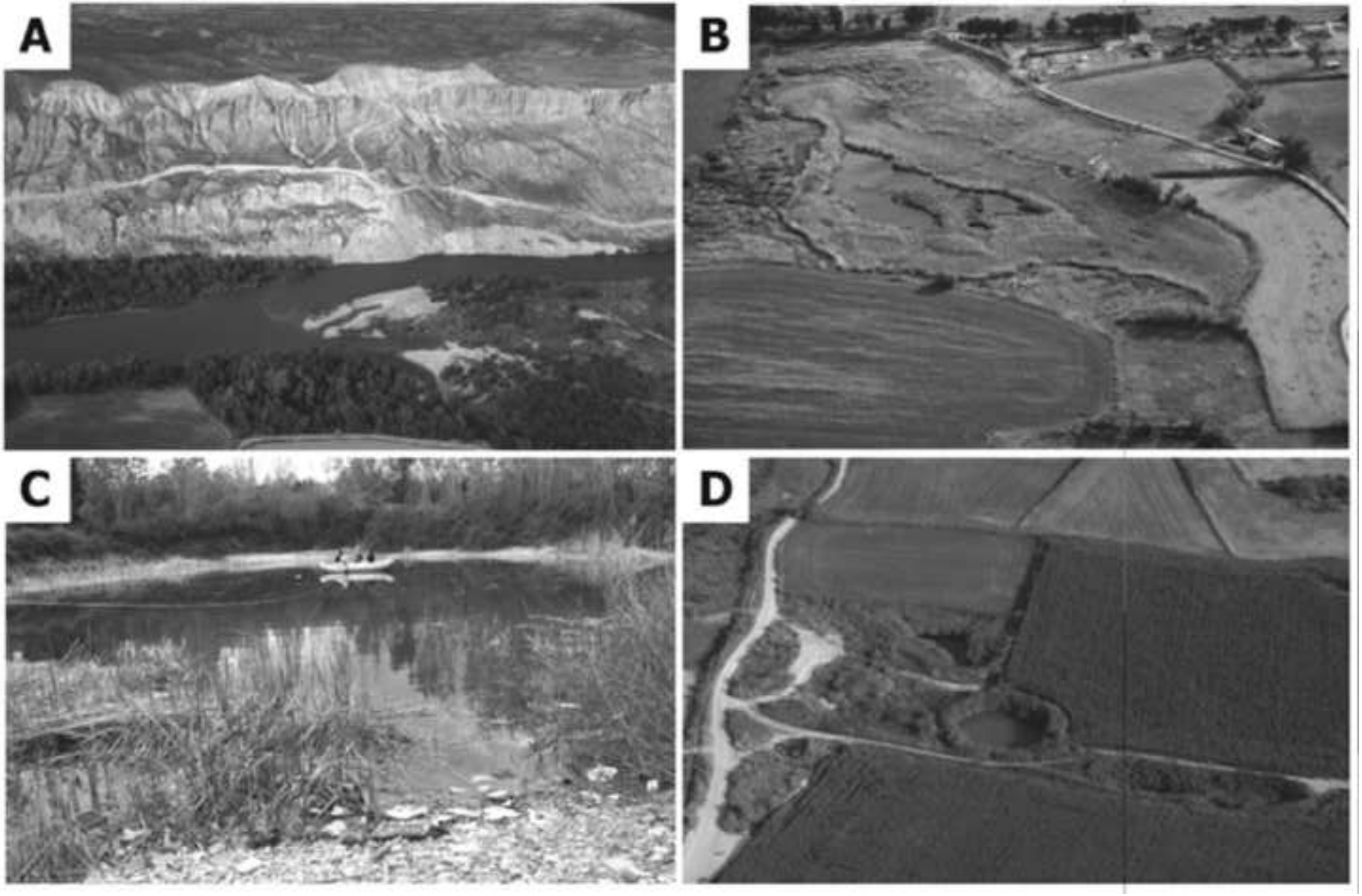

Figure 3

Click here to download high resolution image

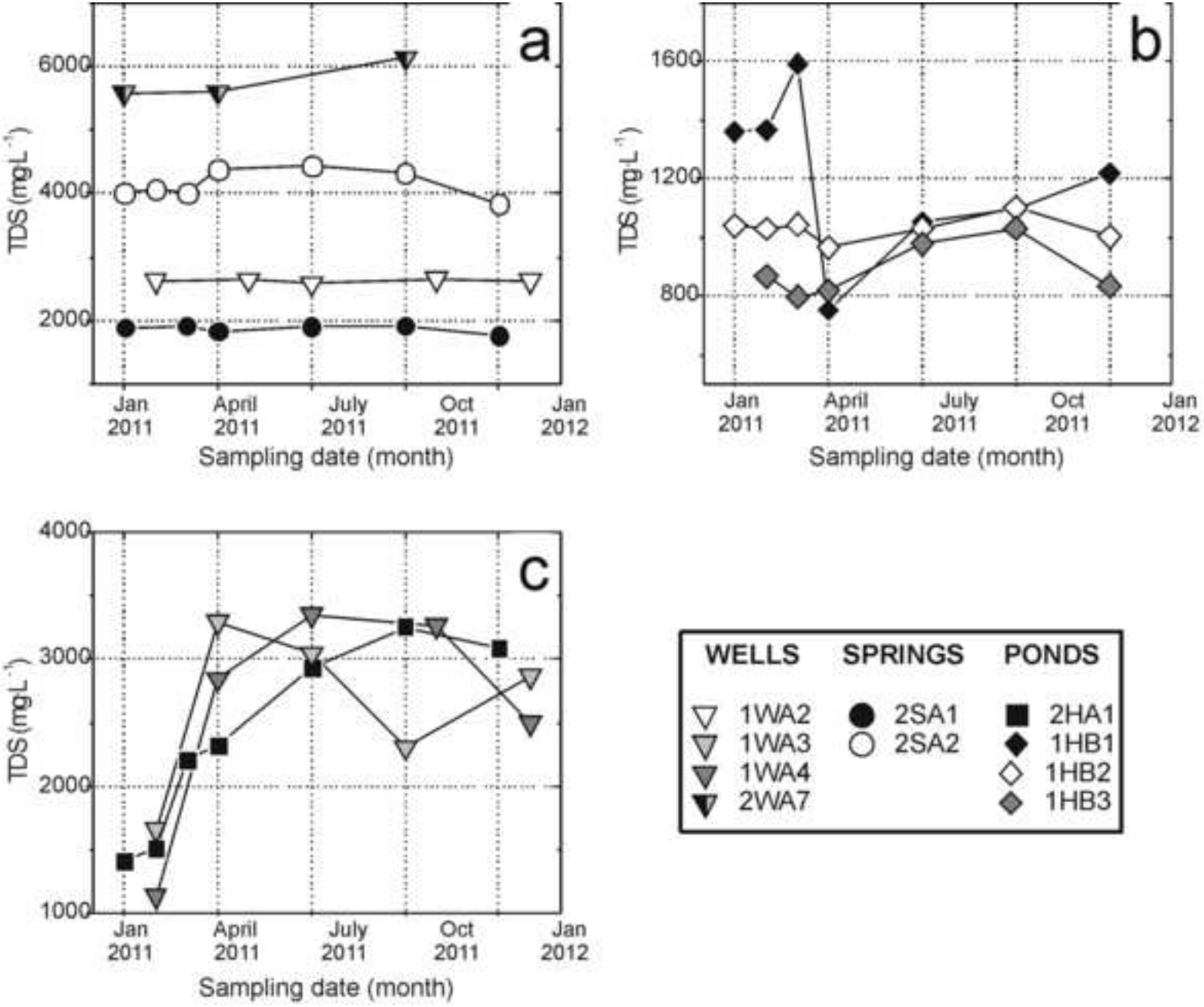

Figure 4

Click here to download high resolution image

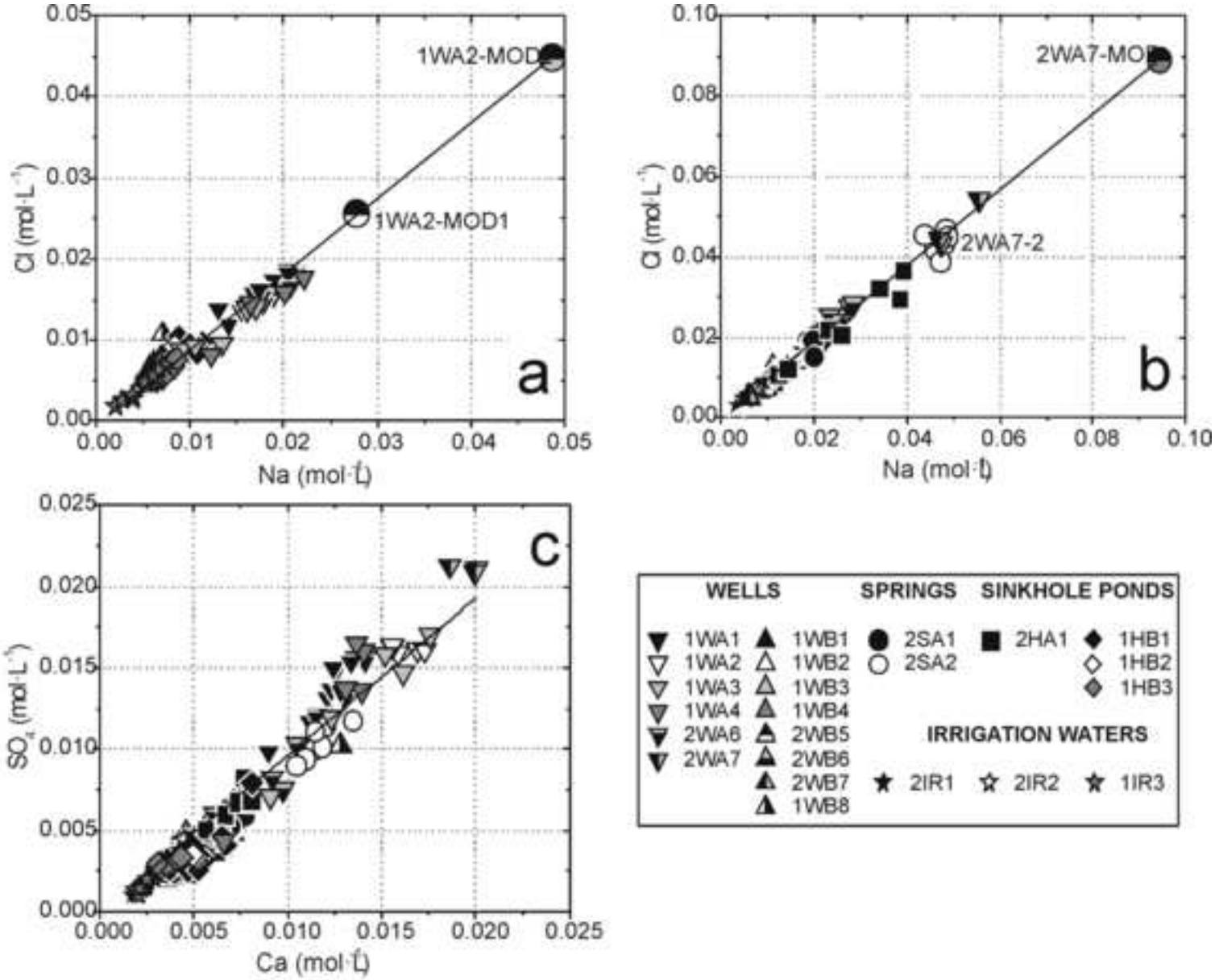

Figure 5

Click here to download high resolution image

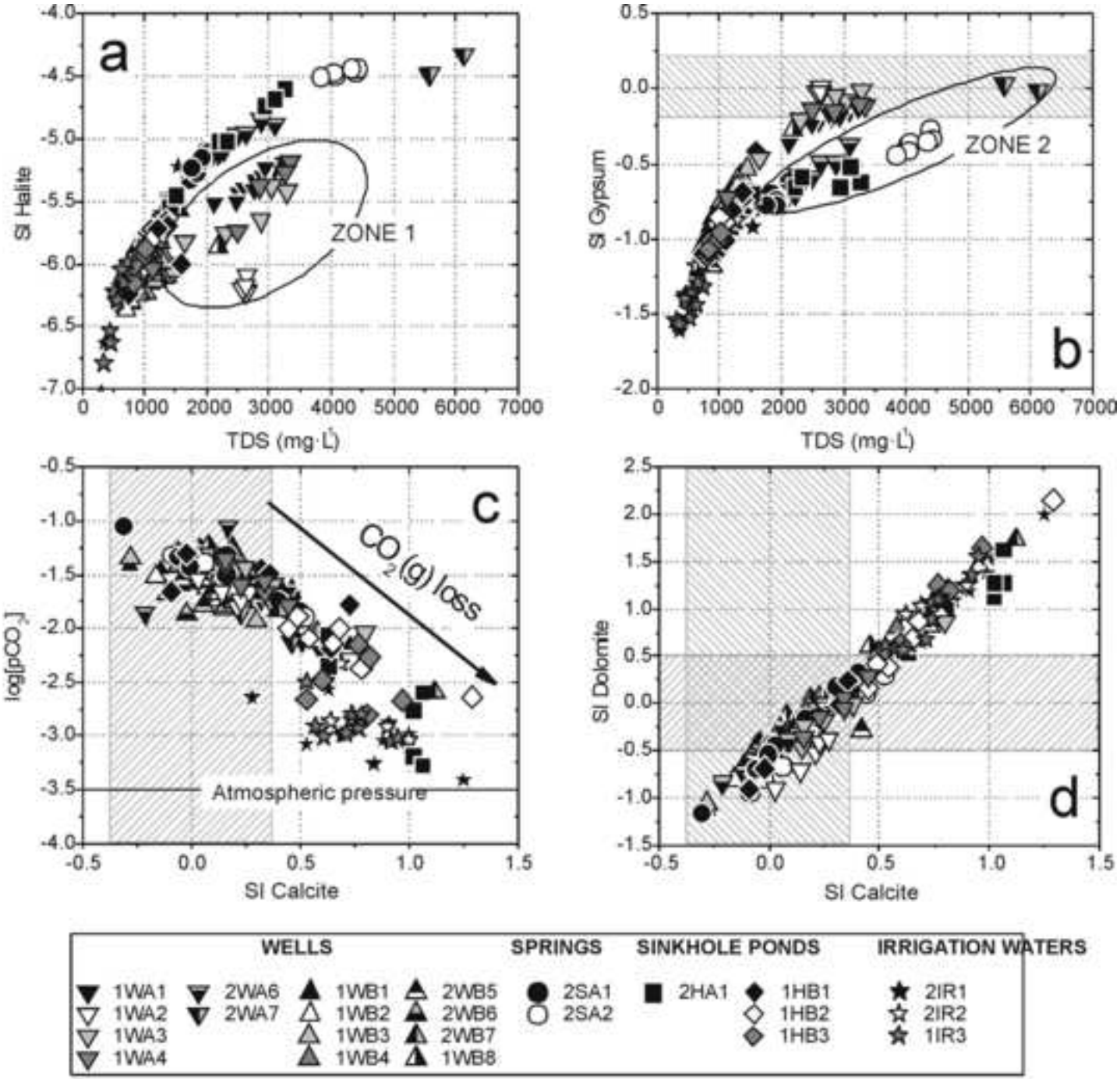

Figure 6

Click here to download high resolution image

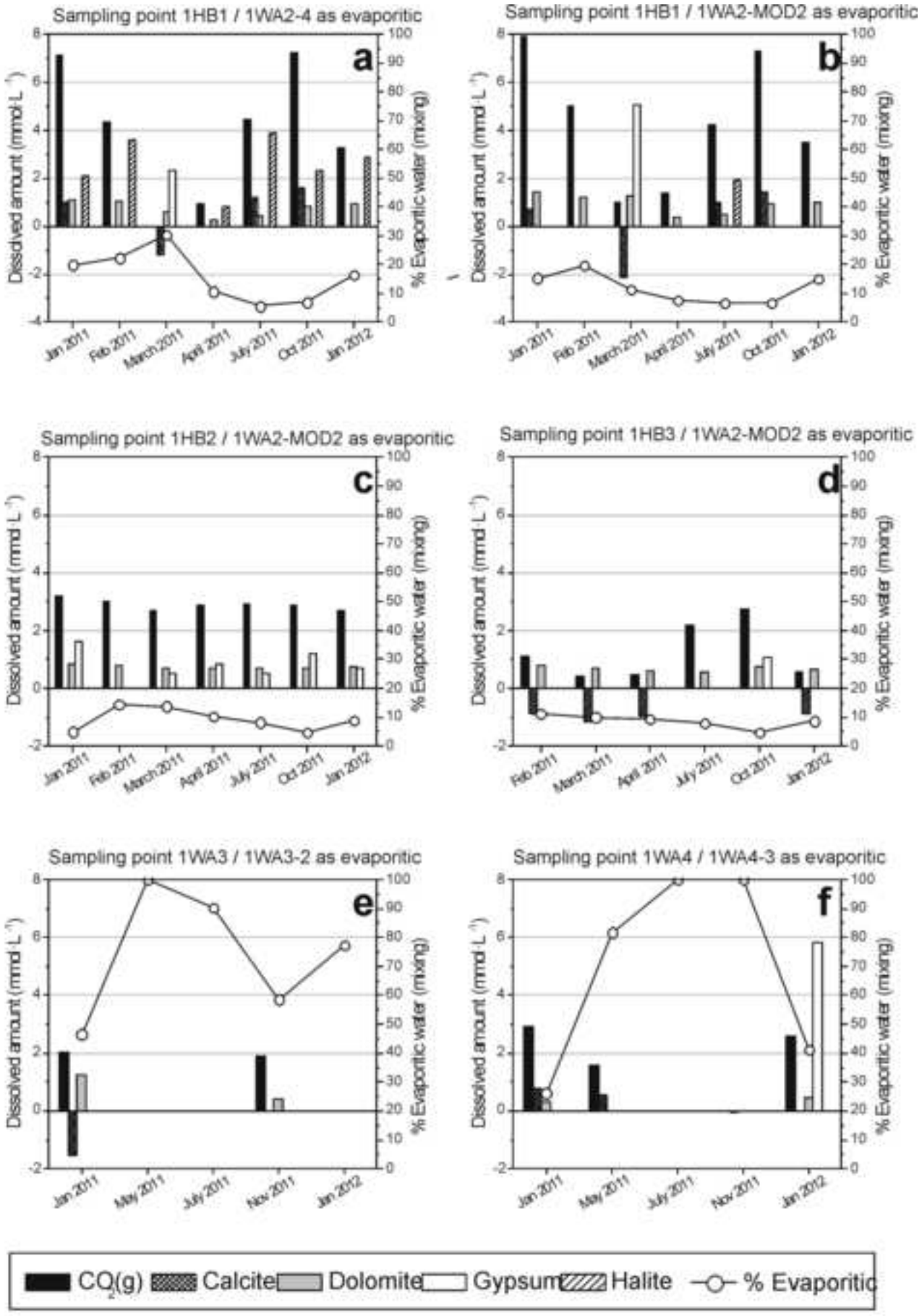

Figure 7

Click here to download high resolution image

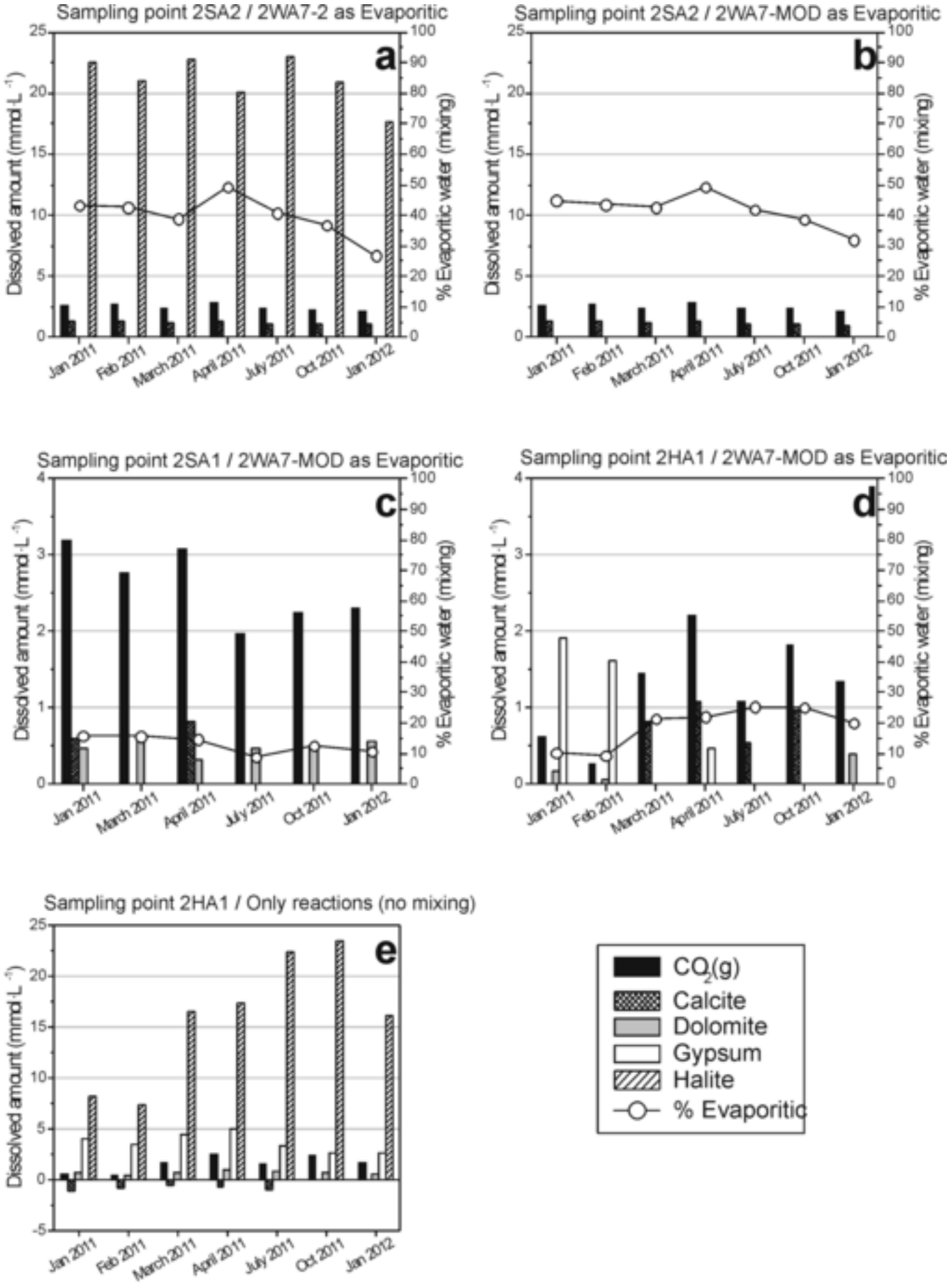

Figure 8

Click here to download high resolution image

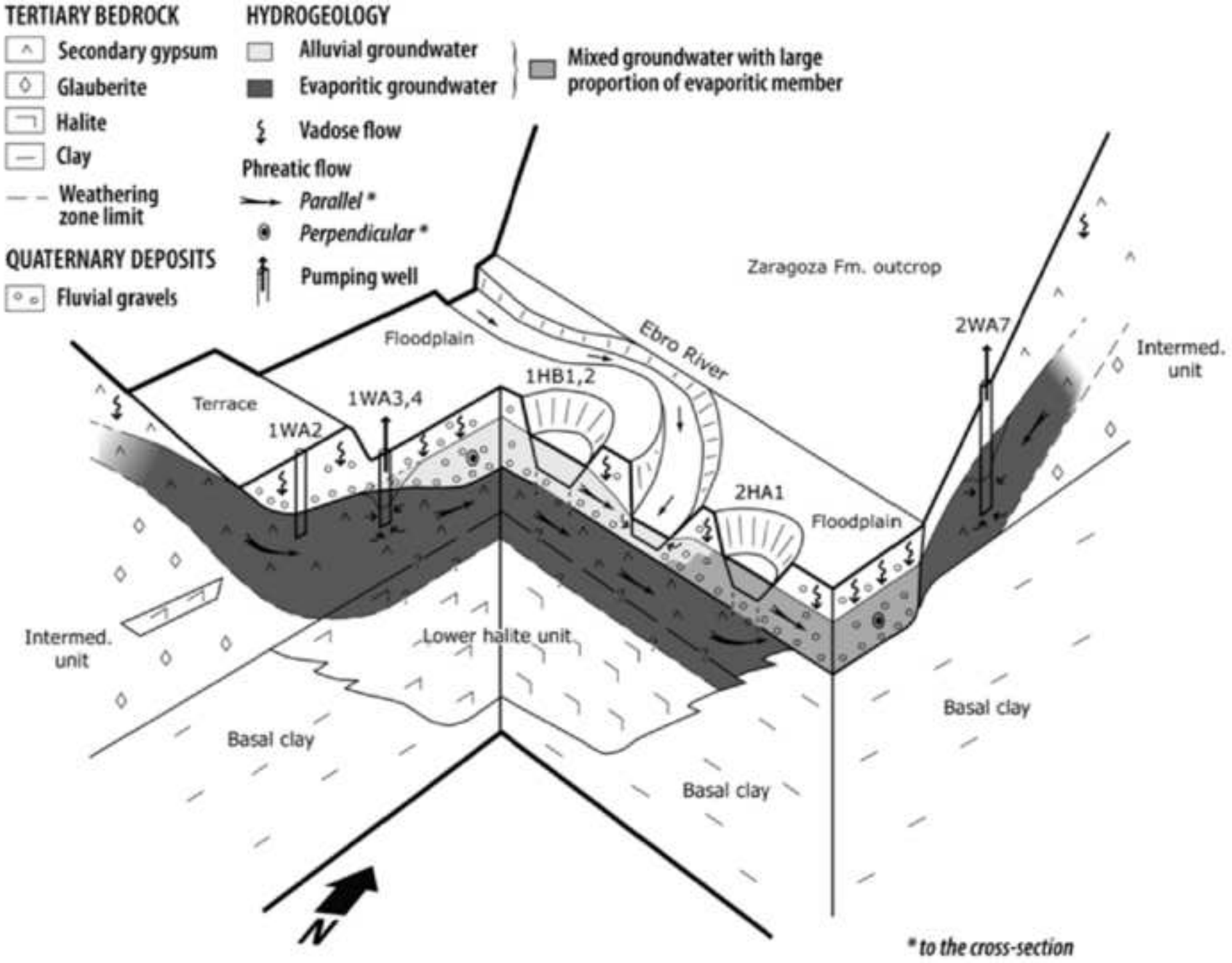

TABLES

Table 1: General features of the sampling points included in this study.

Sampling point	Study zone	Type of water point	Origin of hydrochemical information	Alluvial aquifer thickness (m) (3)	Probable sampled aquifer (4)	Well depth (m) (3)	Watertable average depth (m) (3)	Elevation (m.a.s.l.) (5)
1WA1	1	Pumping well	(1)	10	Mixing	15	2	209
1WA2	1	Pumping well	(2)	37	Evaporitic	70	37.5	239
1WA3	1	Pumping well	(2)	30	Mixing	40	15	218
1WA4	1	Pumping well	(2)	20	Mixing	40	10	207
2WA6	2	Pumping well	(1)	5-10	Mixing	15	5	179
2WA7	2	Pumping well	(2)	n.a.	Evaporitic	101	n.a.	237
1WB1	1	Pumping well	(1)	35	Mixing	38	18	237
1WB2	1	Pumping well	(1)	6	Mixing	14	7	219
1WB3	1	Pumping well	(1)	>52	Alluvial	52	20	229
1WB4	1	Pumping well	(1)	13	Alluvial	14.7	3	205
2WB5	2	Pumping well	(1)	>25	Alluvial	10	4.5	191
2WB6	2	Pumping well	(1)	>12.4	Alluvial	12.4	3.5	187
2WB7	2	Pumping well	(2)	>25	Alluvial	10	4.5	191
1WB8	1	Pumping well	(1)	12	Mixing	23	8	217
2SA1	2	Spring	(1) and (2)	25	Unknown	-	-	181
2SA2	2	Spring	(2)	25	Unknown	-	-	179
2HA1	2	Sinkhole pond	(2)	25	Unknown	-	-	181
1HB1	1	Sinkhole pond	(2)	15	Unknown	-	-	216
1HB2	1	Sinkhole pond	(2)	20	Unknown	-	-	206
1HB3	1	Gravel pit pond	(2)	15	Alluvial	-	-	236
2IR1	2	Irrigation waters from Urdana Ditch	(1) and (2)	-	-	-	-	-
2IR2	2	Irrigation waters from Ebro River	(1)	-	-	-	-	-
1IR3	1	Irrigation waters from Imperial Canal	(1) and (2)	-	-	-	-	-

(1) hydrochemical data obtained from the Ebro Waters Authority (CHE); (2) hydrochemical data obtained from sampling carried out for this study; (3) according to data from CHE water points database (IPA) and/or provided by drilling and engineering geology companies; (4) according to waterlevel data at wells and to alluvial aquifer thickness; (5) elevation data obtained from the CHE Digital Elevation Model (DEM); n.a. : information not available; -: information not applicable for this type of sampling point.

Table 2: Average hydrochemical features of the sampling points included in this study for Zone 1.

Point / Number of samples		TDS [1]	pH	T [2]	Cond [3]	Alk [4]	Ca [5]	Cl [5]	K [5]	Mg [5]	Na [5]	SO_4 [5]	Na/Cl [6]	Ca/SO_4 [6]	Cl/SO_4 [6]
1WA1 / 17	Mean	2874	7.05	17.0	3374	336	497	558	6.3	66	413	1305	1.14	0.92	1.16
	Stdev	327	0.06	0.9	260	19	49	71	1.2	7	57	154	0.08	0.04	0.05
1WA2 / 5	Mean	2622	6.94	15.9	2834	251	650	198	3.6	44	153	1552	1.20	1.00	0.35
	Stdev	27	0.10	1.1	398	27	32	18	0.4	3	9	17	0.11	0.05	0.03
1WA3/ 5	Mean	2633	7.00	16.0	3478	369	564	394	5.4	64	305	1279	1.19	1.08	0.88
	Stdev	657	0.26	1.7	847	28	136	93	0.5	3	79	381	0.14	0.12	0.24
1WA4/ 5	Mean	2618	7.01	16.8	3469	353	492	444	6.3	63	361	1232	1.26	1.04	1.04
	Stdev	897	0.15	1.2	1141	29	128	177	0.5	17	137	473	0.14	0.28	0.3
1WB1 / 28	Mean	773	7.07	16.2	1358	352	163	192	3.2	32	132	226	1.07	1.74	2.31
	Stdev	45	0.12	1.2	97	18	10	15	0.9	4	7	22	0.07	0.14	0.22
1WB2 / 25	Mean	861	7.08	17.4	1474	384	185	205	5.9	35	137	273	1.04	1.63	2.03
	Stdev	58	0.10	1.0	119	30	9	23	0.7	2	11	24	0.07	0.14	0.17
1WB3 / 26	Mean	1204	7.05	16.3	1813	373	250	235	9.7	47	154	479	1.01	1.27	1.36
	Stdev	106	0.13	1.1	171	26	19	25	2.9	5	14	70	0.05	0.12	0.22
1WB4 / 4	Mean	1089	7.05	16.9	1800	409	202	255	5.3	49	163	409	0.98	1.20	1.7
	Stdev	34	0.31	1.4	161	70	12	3	1.8	2	6	44	0.05	0.19	0.17
1WB8 / 5	Mean	1358	6.90	17.2	2052	456	298	270	4.9	74	153	541	0.90	1.36	1.46
	Stdev	477	0.17	1.3	278	70	122	62	2.6	17	16	255	0.15	0.18	0.31
1HB1 / 7	Mean	1205	7.27	11.5	1731	465	229	296	19.9	43	215	387	1.13	1.53	2.44
	Stdev	271	0.37	7.7	350	143	59	69	9.1	10	46	185	0.14	0.36	1.13
1HB2 / 7	Mean	1031	7.62	13.1	1679	380	215	264	6.2	36	185	318	1.09	1.62	2.25
	Stdev	41	0.26	6.1	213	14	11	34	1.4	1	7	10	0.11	0.10	0.32
1HB3 / 6	Mean	887	7.88	15.1	1481	311	148	224	10.0	35	174	286	1.21	1.24	2.12
	Stdev	95	0.16	8.1	261	66	20	33	0.9	3	16	23	0.08	0.10	0.16
1IR3 / 10	Mean	523	8.13	16.7	977	216	90	155	4.1	17	113	144	1.14	1.54	2.88
	Stdev	135	0.13	5.3	219	15	9	60	0.6	4	39	32	0.11	0.23	0.88

[1] TDS: Total dissolved solids (in mg/L); [2] T: temperature (in ^{o}C); [3] Cond: electric conductivity (in $\mu S \cdot cm$); [4] Alk: Alkalinity, as HCO_3^- in mg/L; [5] all values in mg/L; [6] molar ratios

Table 3: Average hydrochemical features of the sampling points included in this study for Zone 2.

Point / Number of samples		TDS [1]	pH	Temp [2]	Cond [3]	Alk [4]	Ca [5]	Cl [5]	K [5]	Mg [5]	Na [5]	SO_4 [5]	Na/Cl [6]	Ca/SO_4 [6]	Cl/SO_4 [6]
2WA6/ 8	Mean	2400	6.99	16.5	3402	393	322	796	5.0	55	538	672	1.06	1.16	3.22
	Stdev	511	0.24	1.1	940	119	70	189	2.3	14	100	169	0.10	0.11	0.41
2WA7 / 3	Mean	5767	7.25	17.6	6543	219	784	1677	10.8	105	1149	2025	1.06	0.93	2.24
	Stdev	314	0.19	0.2	1311	1	33	214	0.9	1	111	20	0.04	0.05	0.27
2WB5 / 19	Mean	1035	7.13	16.5	1641	346	184	261	2.3	32	205	336	1.21	1.32	2.13
	Stdev	82	0.14	2.9	206	28	24	31	0.7	6	26	34	0.05	0.16	0.35
2WB6 / 2	Mean	1419	7.05	19.9	2010	282	229	415	5.2	45	254	462	0.95	1.21	2.44
	Stdev	165	0.07	4.0	269	95	3	55	1.1	3	6	84	0.10	0.20	0.12
2WB7 / 2	Mean	899	7.67	15.5	1482	368	206	183	2.9	36	140	320	1.19	1.54	1.55
	Stdev	16	0.53	1.3	252	3	13	15	0.5	0	6	11	0.15	0.04	0.18
2SA1 / 13	Mean	1922	6.94	16.4	2996	406	265	648	2.7	49	454	492	1.09	1.29	3.58
	Stdev	106	0.21	1.9	326	31	18	70	0.7	3	26	33	0.11	0.07	0.41
2SA2 / 7	Mean	4149	6.96	15.1	6130	350	465	1540	5.2	50	1074	1002	1.08	1.12	4.18
	Stdev	225	0.23	1.3	798	6	39	98	0.7	2	41	99	0.08	0.05	0.35
2HA1/ 7	Mean	2388	7.94	12.7	3647	286	280	832	8.1	38	613	610	1.14	1.11	3.59
	Stdev	741	0.35	7.3	1478	57	38	350	1.5	8	252	112	0.10	0.09	1.16
2IR1 / 10	Mean	1037	8.17	16.2	1809	193	140	342	4.2	21	241	289	1.08	1.24	3.19
	Stdev	440	0.24	6.4	738	19	44	159	1.3	6	116	122	0.08	0.25	0.45
2IR2 / 5	Mean	891	8.02	15.2	1534	252	138	251	4.1	30	181	292	1.11	1.15	2.31
	Stdev	248	0.26	8.3	330	23	26	76	1.2	6	60	82	0.05	0.13	0.08

[1] TDS: Total dissolved solids (in mg/L); [2] T: temperature (in °C); [3] Cond: electric conductivity (in µS·cm); [4] Alk: Alkalinity, as HCO_3^- in mg/L; [5] all values in mg/L; [6] molar ratios

Table 4: Pearson correlation coefficients between the different variables included in this study.

	TDS	pH	Temp	Cond	Alk (HCO_3^-)	Ca	Cl	K	Mg	Na	SO_4	Sr
TDS	1											
pH	-0.26	1										
Temp	0.03	-0.15	1									
Cond	0.95	-0.23	0.04	1								
Alk (HCO_3^-)	-0.04	-0.59	-0.02	0.03	1							
Ca	0.90	-0.38	0.05	0.78	0.01	1						
Cl	0.88	-0.13	0.02	0.93	-0.01	0.59	1					
K	0.12	0.02	-0.26	0.06	0.15	0.16	0.04	1				
Mg	0.76	-0.49	0.05	0.67	0.29	0.81	0.54	0.25	1			
Na	0.89	-0.11	-0.01	0.94	-0.03	0.61	0.99	0.04	0.53	1		
SO_4	0.90	-0.30	0.05	0.77	-0.09	0.98	0.58	0.15	0.79	0.60	1	
Sr	0.86	-0.61	0.19	0.72	-0.09	0.99	0.52	-0.09	0.84	0.53	0.97	1
Si	0.52	-0.66	0.09	0.44	0.48	0.67	0.25	0.29	0.72	0.27	0.64	0.57

Table 5: Hydrochemistry of the samples used as evaporitic end members in the mixing + mass balance calculations.

Sample	Zone	pH	T [1]	Alk [2]	Ca [3]	Cl [3]	Mg [3]	Na [3]	SO_4 [3]
1WA2-4	1	7.01	15.8	254	624	228	48	159	1564
1WA2-MOD1	1	7.01	15.8	254	624	911	48	637	1564
1WA2-MOD2	1	7.01	15.8	254	624	1594	48	1116	1564
1WA3-2	1	6.74	17.4	347	705	489	68	372	1634
1WA4-3	1	7.16	17.3	326	564	628	79	509	1536
2WA7-2	2	7.03	17.5	218	801	1579	104	1082	2004
2WA7-MOD	2	7.03	17.5	218	801	3158	104	2165	2004

[1] T: temperature (in ^{o}C); [2] Alk: Alkalinity, as HCO_3^- in mg/L; [3] all values in mg/L